Delft University of Technology
Department of Civil Engineering
Group of Fluid Mechanics

Diffraction in a spectral wave model

- final report -

February 1997

N. Doorn

Delft University of Technology
Department of Civil Engineering
Group of Fluid Mechanics

Diffraction in a Spectral Wave Model

- final report -

Supervisors:
prof.dr.ir. J.A. Battjes
dr.ir. L.H. Holthuijsen
dr.ir. N. Booij

Student
N. Doorn (192379)

Delft, February 1997

ABSTRACT

Waves that approach the coast and encounter obstacles such as small islands, rocks or breakwaters may be reflected backwards and in lateral directions, but the wave crest may also bend around the obstacle. This phenomenon can be described with refraction-diffraction models based on the Boussinesq equation or the mild-slope equation of Berkhoff. However, these models are computationally very demanding since they require a high spatial resolution. Moreover, physical phenomena such as wind generation or depth induced breaking are not readily accounted for. Inclusion of diffraction in a spectral wave model would eliminate these drawbacks. Similar to refraction the effect of diffraction can be represented as a transport of wave energy through spectral space (in the directional domain). Two ad hoc proposals are made to include diffraction in the model SWAN, which is a fully spectral model based on the action balance equation. The first proposal to describe this diffraction-induced turning rate is derived from the mild-slope equation for monochromatic, long-crested waves. It depends on the second order spatial derivative of the wave amplitude. Adding the diffraction term made the model unstable. The second proposal to describe the diffraction-induced turning rate is based on the first-order spatial gradient of the wave field. The transport of wave energy along the wave crests is proportional to the first-order derivative of the energy along the crest. The model is tested for three different cases: the academic case of monochromatic, unidirectional waves near a semi-infinite breakwater, a realistic harbour and the Bay of Viano do Castelo (Portugal). In areas with considerable wave motion the influence of diffraction is relatively unimportant. In other regions the gradient-approach for diffraction seems to give a realistic estimate for the wave field.

SAMENVATTING

Golven die de kust naderen en in aanraking komen met een obstakel, zoals een klein eiland of een golfbreker kunnen gereflecteerd worden, maar ook zijdelings uitwaaieren. Dit verschijnsel kan beschreven worden met een gecombineerd refractie-diffractie model, gebaseerd op de vergelijking van Boussinesq of de 'mild-slope' vergelijking van Berkhoff. De rekentijd van deze modellen is echter erg groot, gezien de benodigde hoge resolutie in de geografische ruimte (x- en y- richting). Bovendien kunnen met deze modellen verschijnselen zoals de energieoverdracht tussen golven en wind of het breken van golven op een helling niet goed gesimuleerd worden. Modellen die gebaseerd zijn op de energiebalans-vergelijking hebben deze nadelen niet. Deze modellen hebben echter het nadeel dat diffractie niet gesimuleerd wordt en dat de uitkomsten direct achter een obstakel dus niet nauwkeurig zijn. In dit afstudeerwerk is een poging gedaan om diffractie op te nemen in het spectrale golfmodel SWAN, dat is gebaseerd op de actie balans vergelijking.

Net als refractie kan diffractie worden gezien als een transport van golfenergie in de spectrale ruimte (in het richting-domein). Op twee manieren is geprobeerd de richtingsverandering te beschrijven. Het eerste voorstel is gebaseerd op de 'mild-slope' vergelijking die is afgeleid voor monochromatische, langkammige golven. De richtingsverandering hangt in dit geval af van de tweede afgeleide van de golfamplitude. Het is echter niet gelukt met dit model stabiele uitkomsten te krijgen. Het tweede voorstel is gebaseerd op de ruimtelijke (eerste orde) gradiënt van het golfveld. Het energietransport langs de golfkam is evenredig met de gradiënt van de golfenergie langs de kam. Het model is getest voor drie situaties: de academische test van monochromatische, rechtkammige golven bij een half-oneindige golfbreker, een realistische haven en de baai van Viano do Castelo (Portugal). In gebieden met een aanzienlijke golfbeweging is de invloed van diffractie relatief onbelangrijk. In andere gebieden bleek het model realistische uitkomsten te geven.

TABLE OF CONTENTS

Abstract i

Samenvatting ii

Table of contents iii

INTRODUCTION 1

BASIC EQUATIONS 4

NUMERICAL FORMULATION 7

Numerical Scheme for the propagation in geographical space 7

Numerical Scheme for the propagation in spectral space 7

Boundary conditions 8

Stability 10

METHOD OF THE STUDY 11

Academic tests 11

Harbour 18

Viano do Castelo 21

CONCLUSIONS 24

Acknowledgements 26

References 27

Notation 28

Appendix I : Physical Background

Appendix II : Numerical Background

Appendix III : Stability Analysis

Appendix IV : Attempts to make the model stable

Appendix V : Sommerfeld-solution

INTRODUCTION

Numerical wave propagation models are nowadays widely used in engineering practise to predict wave behaviour in coastal regions. These models simulate the transformation of wave characteristics from the location where wave data are collected to the site of concern. A large number of numerical codes have been developed with a varying degree of approximation in the description of several physical processes, such as shoaling, refraction, diffraction, wave-current interaction, etc.. One can distinguish between two main kinds of wave propagation models:

1) the combined refraction-diffraction models;
2) models based on the wave energy or action balance equation.

The process of difraction can be described by the two-dimensional Helmholtz equation:

$$\nabla^2\phi+k^2\phi=0 \qquad (1)$$

with $\phi(x,y)=A(x,y)e^{-i\omega t}$ denoting the complex two-dimensional wave potential function at the free surface, A(x,y) its amplitude, ω the angular frequency and k the wave number. Analytical solutions can be obtained only for highly idealized conditions, such as a constant depth and obstacles with a special geometry (see also Appendix V). For slowly varying depth the wave number k can be assumed to be the same as for a horizontal bed. Based on this idea Berkhoff (1976) derived a two dimensional partial differential equation to describe the combined effect of refraction and diffraction using the so called mild-slope approximation :

$$\nabla c_g c(\nabla\phi)+\omega^2\frac{c_g}{c}\phi=0 \qquad (2)$$

with c and c_g the local phase and group velocities respectively. The combined refraction-diffraction models for monochromatic unidirectional waves are based on the mild-slope equation.

Since the mild-slope equation is elliptical, boundary conditions along the entire boundary are needed and the equation is solved simultaneously for all interior points. In order to obtain a numerical solution a great amount of computing time and storage is needed. To overcome this problem parabolic models have been developed (Biesel, 1972; Radder, 1979), which are easier to solve numerically since the parabolic approach does not need simultaneous solution at all grid points, but allows a marching method. Since then parabolic type equations have been extended to include more physical processes such as non-linear effects, the effects of slowly varying currents, dissipation due to wave breaking or wave-bottom interaction and wave growth due to wind (Kirby and Dalrymple, 1983; Booij, 1981; Dingemans, 1985).

The parabolic model however has some disadvantages. The waves must propagate in a principal direction, since the diffraction effects are restricted to one direction (perpendicular to the direction of propagation) and

the models deal with regular waves only. The representation of irregular waves by monochromatic waves leads to significant deviation of the actual wave conditions (Vincent and Briggs, 1989). Panchang et al. (1990) pointed out that linear superposition of the results from a monochromatic refraction-diffraction model can simulate the irregular sea state satisfactorily as long as non-linear effects between frequencies are small. This linearity is used in the combined refraction-diffraction model CREON (Gao et al., 1993), in which the spectrum is parameterized in frequency domain, i.e. a mean frequency is used in the model instead of a full discretization of the frequency spectrum.

The spectral wave models are based on the wave action (or energy) balance equation describing the propagation, generation and dissipation of the wave action density through the four dimensional (x,y,θ,σ) - space:

$$\frac{\partial}{\partial t}N(\sigma,\theta)+\nabla_{x,y}[\underline{c}\ N(\sigma,\theta)]+\frac{\partial}{\partial\sigma}[c_\sigma N(\sigma,\theta)]+\frac{\partial}{\partial\theta}[c_\theta N(\sigma,\theta)]=\frac{S(\sigma,\theta)}{\sigma} \qquad (3)$$

in which N(σ,θ) represents the action density, defined as the ratio of the energy density E(σ,θ) to the intrinsic frequency (σ), as a function of this intrinsic frequency and the spectral wave direction. The left hand side of Eq. 3 represents the local rate of change of the action density, propagation in geographic space (term $\nabla_{x,y}$), shifting of the intrinsic frequency due to variations in depth and currents (term with $\partial/\partial\sigma$) and refraction (term with $\partial/\partial\theta$). The right hand side represents the different processes of generation and dissipation of waves. If no currents are present and $\partial d/\partial t = 0$ action is not propagated in frequency space. In that case the action balance reduces to an energy balance. Since the residence time of the waves in coastal areas is usually short compared to the timescale of variations in the wave boundary conditions, it seems justified to remove time as an independent variable (i.e. to make the model stationary) for coastal applications. The resulting action balance equation reads:

$$\frac{\partial}{\partial x}[c_x N(\sigma,\theta)]+\frac{\partial}{\partial y}[c_y N(\sigma,\theta)]+\frac{\partial}{\partial\theta}[c_\theta N(\sigma,\theta)]=\frac{S(\sigma,\theta)}{\sigma} \qquad (4)$$

The spectral wave models can be used in case the changes of wave properties on a scale of a wavelength are weak and therefore can be neglected. This is the case in regions of slowly varying depth and current. Because of the slow variations of the phase-averaged wave-properties the wave field can be treated as quasi-uniform. A spectral model with full discretization in frequency and directional domain can reliably represent various physical processes. These models have been used extensively for the prediction of the properties of ocean waves (the WAM-model (WAMDI, 1988)) and the wave field of shelf seas (the model WAVEWATCH (Tolman, 1991)). In near-shore areas a high resolution in geographical domain is required due to the more rapid depth variation. For numerical schemes that are subjected to the Courant stability criterion this implies also small time increments of the numerical integration.

One of the fundamental limitations of the spectral wave models is the absence of an expression representing the diffraction effects. Therefore, the wave field generated by these models will generally not be accurate immediately behind obstacles.

Resio (1988) developed a steady-state spectral model in which diffraction is modelled as a diffusion process. First the wave field without diffraction is determined. By means of a convolution filter the wave energy is redistributed in geographical space. Diffraction is not simulated as a redirection of the waves.

In the model PROPS Rivero (1993) uses an expression for the wave number, which is exact within the mild-slope approximation:

$$(\nabla\psi)^2 = k^2\left(1 + \frac{\nabla(cc_g\nabla\phi_0)}{k^2 cc_g\phi_0}\right) \qquad (5)$$

The effects of combined refraction and diffraction are included in Eq. 5. However, the propagation in directional domain (the term with $\partial/\partial\theta$ in Eq. 3) is not represented in the model PROPS. Therefore both refraction and diffraction are not simulated as a redirection of the waves.

In the present study an attempt is made to introduce diffraction into the SWAN model in two different ways. In both formulations diffraction is represented as a propagation of wave energy through spectral space (in directional domain). In the first formulation the diffraction-induced turning rate is derived from the mild-slope equation. However the numerical techniques in the SWAN model are specifically designed for the energy balance equation which is normally a first-order differential equation. Adding the diffraction term increases the order of the equation and the model became numerically unstable. In Appendix IV the attempts to make the model stable are given. The second proposal is based on a transport of wave action along the wave crests proportional to the spatial gradient of the wave action normal to the propagation direction of the waves. This gradient approach is compared with the solutions of Goda (1978). The model is also applied to a realistic harbour and an actual field case.

BASIC EQUATIONS

Both refraction and diffraction can be seen as energy propagation in the directional domain. Whereas refraction is caused by the variations in the phase speed along the wave crests (due to varying depths or currents), diffraction is caused by a variation of the wave amplitude in the horizontal plane. The combined effect of refraction and diffraction can be described by the mild-slope equation for monochromatic, unidirectiona waves (Berkhoff, 1976):

$$\nabla c_g c(\nabla\phi)+\omega^2\frac{c_g}{c}\phi=0 \tag{6}$$

Substitution of:

$$\phi_0=a(x,y)e^{i\psi(x,y)} \tag{7}$$

into the mild-slope equation and equating the real part to zero gives the following equation for the phase function ψ(x,y):

$$|\nabla\psi|^2=k^2\left(1+\frac{\nabla(c_g c\nabla a)}{k^2 c_g c a}\right) \tag{8}$$

or for brevity:

$$|\boldsymbol{K}|=k\sqrt{1+\delta} \quad in\ which \quad \delta=\frac{\nabla\cdot(cc_g\nabla a)}{k^2 cc_g a} \tag{9}$$

The first term in the right-hand side of Eq. 8 represents the refraction effects, whereas diffraction is represented by the second term. In case of constant depth Eq. 8 equals the expression for the wave number derived by Battjes (1968) :

$$|\nabla\psi|^2=k^2\left(1+\frac{a_{xx}+a_{yy}}{k^2 a}\right) \tag{10}$$

The conventional equation for the phase function ψ(x,y) is:

$$|\nabla\psi|^2=k^2 \tag{11}$$

The solution of Eq. 11 can be obtained by integration of the following set of first-order differential equations:

$$\begin{aligned} \frac{dx}{dt}&=\frac{c_g}{k}\frac{\partial\psi}{\partial x} \quad ; \quad \frac{dy}{dt}=\frac{c_g}{k}\frac{\partial\psi}{\partial y} \\ \frac{d}{dt}\left(\frac{\partial\psi}{\partial x}\right)&=-\frac{\partial\sigma}{\partial d}\frac{\partial d}{\partial x} \quad ; \quad \frac{d}{dt}\left(\frac{\partial\psi}{\partial y}\right)=-\frac{\partial\sigma}{\partial d}\frac{\partial d}{\partial y} \end{aligned} \tag{12}$$

Denoting the direction of the vector ∇ψ as θ, the expressions for rectilinear propagation are:

$$\frac{dx}{dt}=c_g\cos\theta \quad ; \quad \frac{dy}{dt}=c_g\sin\theta \tag{13}$$

Combination of Eq. 12 and 13 gives the following expression for the propagation speed in directional domain:

$$c_\theta=\frac{c_g}{k}\frac{\partial k}{\partial m} \tag{14}$$

in which m is a coordinate along the wave crest (see Fig. 1):

$$\frac{\partial}{\partial m}(\ldots)=-\sin\theta\frac{\partial}{\partial x}(\ldots)+\cos\theta\frac{\partial}{\partial y}(\ldots) \tag{15}$$

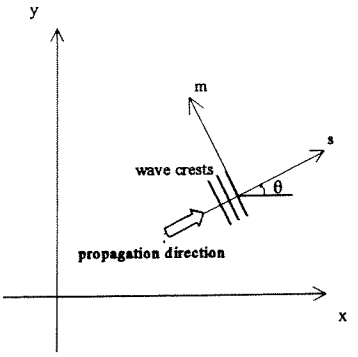

Figure 1. Coordinate system

By substitution of the wave number derived from the mild-slope equation, denoted by **K**, into Eq. 14 the effects of refraction as well as diffraction are represented:

$$c_\theta = \frac{c_g}{K}\frac{\partial K}{\partial m} \tag{16}$$

Spectral formulations for diffraction

As said before the mild-slope equation is derived for monochromatic, unidirectional waves. A spectral formulation is not available. Two proposals are made for a spectral formulation for the diffraction-induced turning-rate.

Mild-slope approach

In the first formulation the diffraction-induced turning rate is derived from the mild-slope equation. The mild-slope equation is derived for monochromatic, long-crested waves. However, the second-order derivatives are normalized with the amplitude itself, so that the expression is linear. Therefore it seems possible to replace the second-order derivatives by a normalized second-order derivative of the square root of the energy density per spectral wave component. For each spectral component the wave number **K** can be determined and with Eq. 13 the diffraction induced turning-rate can be calculated.

The wave number **K** depends on the second-order spatial derivative of the wave amplitude, as described by Eq. 8. Therefore the distribution of the wave energy needs to be known before the wave number can be calculated. An iterative procedure is used. First the wave field is computed without the proposed diffraction-induced turning rate. Then the wave number based on the mild-slope equation can be determined. The computations are repeated with the new values for the wave number. The iteration is terminated when the significant wave height and the mean wave period have changed less than a certain (user-provided) percentage.

Gradient approach

An alternative, more pragmatic formulation is based on the first-order derivative of the wave action. From the foregoing it appears that the spatial variation of the wave field seems to be some indicator for the diffraction-induced directional shift c_θ. Instead of using the second-order derivatives of the wave amplitude, the (first-order) gradient of the wave field along the wave crest is used. It seems plausible that the spatial gradient of the action density normal to the direction of propagation:

$$\frac{\partial N}{\partial m} \tag{17}$$

is some indicator for diffraction. Analogous to Eq. 14 it is proposed to represent the diffraction-induced turning rate c_θ^* by the (normalized) product of this gradient and the geographical propagation velocity:

$$c_\theta^* = -\gamma \frac{c_g}{N} \frac{\partial N}{\partial m} \tag{18}$$

The coefficient γ is used for tuning the gradient approach. The turning-rate is computed per spectral component. The purpose of this approach is not to produce an accurate representation of diffraction but to spatially smooth the wave conditions in areas with strong gradients in the wave field. The reformulated action balance reads:

$$\frac{\partial N}{\partial t} + \nabla_{x,y}[\underline{c}\ N] + \frac{\partial}{\partial \sigma}[c_\sigma N] + \frac{\partial}{\partial \theta}[(c_\theta - \gamma \frac{c_g}{N} \frac{\partial N}{\partial m})N] = \frac{S}{\sigma} \tag{19}$$

where diffraction is represented by the fifth term as a transport of energy from one direction to another at a rate $\gamma c_g(\partial N/\partial m)$.

NUMERICAL FORMULATION

Numerical Scheme for the propagation in geographical space

In SWAN a so called four sweep method is used. The directional domain is divided into four quadrants. First the state in grid point (x_i,y_i) is determined from two up-wave points (x_{i-1},y_i) and (x_i,y_{i-1}). This stencil covers the propagation of action density within a sector of 0°-90°, in the entire geographic space. A first-order upwind scheme is used to ensure unconditionally stable integration. Now the stencil is rotated over 90° and the same procedure is repeated for the propagation of action density within the sector 90°-180°. The stencil is rotated twice more to cover all four quadrants. The influence of refraction (and therefore waves possibly shifting from one quadrant to another) is taken into account by repeating the computations until the convergency conditions are fulfilled (see also Appendix II):

a) Relative or absolute change in significant wave height less than a user-defined limit, and

b) Relative or absolute change in mean wave period less than a user-defined limit, and

c) conditions a) and b) are fulfilled in more than a user-defined percentage (e.g. 97%) of all wet grid points.

Numerical Scheme for the propagation in spectral space

By means of a numerical coefficient α the user can choose between an implicit central difference scheme ($\alpha = 0$), which has the largest accuracy (no numerical diffusion) and an implicit upwind difference scheme ($\alpha = 1$), which is more robust (but more diffusive), for the propagation in σ- and θ-space. The computations are carried out with a central difference scheme, to minimize the numerical diffusion. To compare the stability of both numerical schemes the compuations are also carried out with an upwind scheme. No difference between the results could be found. Since the central difference scheme has no numerical diffusion this implies that the numerical diffusion for the upwind scheme can be neglected (for the purpose of this study). Moreover, the model is not significantly more robust if the diffraction-induced turning rate is calculated with an upwind scheme. The results presented in the next section are obtained with a central difference scheme for the propagation in θ-domain.

Mild-slope approach

The wave number is calculated with a central difference scheme. In stead of the wave amplitude the square root of the action density is taken to compute the second derivative in geographical domain:

$$1+\frac{a_{xx}+a_{yy}}{k^2 a} = 1+\frac{\sqrt{N_{x_i+1}}-2\sqrt{N_{x_i}}+\sqrt{N_{x_i-1}}}{k^2\sqrt{N_{x_i}}\,\Delta x^2} + \frac{\sqrt{N_{y_i+1}}-2\sqrt{N_{y_i}}+\sqrt{N_{y_i-1}}}{k^2\sqrt{N_{y_i}}\,\Delta y^2} \qquad (20)$$

in which:

$$\overline{N_{x_i}}=\frac{N_{x_i+1}+2N_{x_i}+N_{x_i-1}}{4} \quad and \quad \overline{N_{y_i}}=\frac{N_{y_i+1}+2N_{y_i}+N_{y_i-1}}{4} \tag{21}$$

Gradient-approach

The propagation in directional domain is calculated with a central difference scheme:

$$\frac{\partial}{\partial\theta}(c_\theta N-\gamma c_g\frac{\partial N}{\partial m})=\frac{(1+\alpha)[c_\theta N-c_g\frac{\partial N}{\partial m}]_{\theta_i+1}-(2\alpha)[c_\theta N-c_g\frac{\partial N}{\partial m}]_{\theta_i+1}-(1-\alpha)[c_\theta N-c_g\frac{\partial N}{\partial m}]_{\theta_i+1}}{2\Delta\theta} \tag{22}$$

The spatial gradient can be written as:

$$c_g\frac{\partial N}{\partial m}=-c_y\frac{\partial N}{\partial x}+c_x\frac{\partial N}{\partial y} \tag{23}$$

Eq. 23 is calculated with a first-order upwind scheme:

$$\gamma c_x\frac{\partial N}{\partial y}=\gamma c_x\frac{N_{y_i}-N_{y_i-1}}{\Delta y} \quad and \quad \gamma c_y\frac{\partial N}{\partial x}=\gamma c_y\frac{N_{x_i}-N_{x_i-1}}{\Delta x} \tag{24}$$

Boundary conditions

Although the grid is essentially four-dimensional (x,y,σ,θ) it can be subdivided into two different grids, i.e. a two-dimensional grid for the geographical space (x,y) and a two-dimensional grid for the spectral space (σ,θ).

The computational grid in geographical space is rectangular. The four-sweep technique allows waves to propagate from all directions. Therefore boundary conditions must be present at all boundaries. Along closed boundaries (i.e. coast lines) the wave energy is totally absorbed (no reflection). At the open (sea) boundaries, wave energy propagates out of the computational area (no reflection) or it enters the computational area with the user-provided boundary conditions.

If the user is confident that no energy will occur outside a certain directional sector then the computations by SWAN can be limited to the directional sector that does contain energy. If the computations are carried out with a directional sector instead of a full circle the boundaries of the θ-domain are totally absorbing, i.e. there is an undisturbed wave propagation for waves leaving the computational grid in θ-domain and there is no incoming waves energy at the boundaries of the θ-domain. Since the computations are made in the absence of currents there is no transport of action density in frequency domain.

Mild-slope approach

The wave number **K**, derived from the mild-slope equation, contains a second-order spatial derivative of the action density. Because the propagation velocity in directional domain contains a first derivative of this

wave number **K**, the term in the action balance equation is of the third order. This means that three boundary conditions are necessary at the boundaries of the geographical domain. Apart from the one boundary condition necessary for the propagation term, the two other boundary conditions in x-direction are assumed:

$$\frac{\partial N}{\partial x}=0 \quad and \quad \frac{\partial^2 N}{\partial x^2}=0 \tag{25}$$

and in y-direction:

$$\frac{\partial N}{\partial y}=0 \quad and \quad \frac{\partial^2 N}{\partial y^2}=0 \tag{26}$$

These conditions imply that diffraction is neglected at the boundaries of the computational domain.

Internal boundaries

The diffraction-induced turning rate is calculated as a spatial derivative of the wave number with a first order upwind scheme:

$$c_\theta=\frac{c_g}{K}\frac{\partial K}{\partial m}=\frac{c_g}{K}\left[-\sin\theta\frac{K_{x_i}-K_{x_i-1}}{\Delta x}+\cos\theta\ \frac{K_{y_i}-K_{y_i-1}}{\Delta y}\right] \tag{27}$$

At internal boundaries, i.e. 'dry' grid points inside the computational area, the depth is negative. Since the wave number is not defined in 'dry' grid points the diffraction-induced turning rate can not be calculated in the first grid point downwave of a 'dry' grid point. In these grid points the turning rate is assumed to be equal to zero.

Gradient-approach

In geographical domain no extra boundary conditions are necessary. In θ-domain one extra boundary is necessary. For waves leaving the θ-domain the spatial gradient of action density is assumed constant in θ-domain. This results in the following extra boundary condition for waves leaving the directional domain:

$$\frac{\partial}{\partial\theta}\left(\gamma c_g\frac{\partial N}{\partial m}\right)=0 \tag{28}$$

For waves entering the θ-domain the spatial gradient of action density is equal to zero, which results in the following extra boundary condition:

$$\left(\frac{\partial N}{\partial m}\right)=0 \tag{29}$$

For this approach the internal boundaries have no influence on the numerical scheme. In 'dry' grid points the wave action is defined (N = 0), and the spatial gradient can be calculated.

Stability

From a stability analysis it follows that the ratio of γ to ΔΘ is an indicator for the stability of the numerical formulation. Due to the necessary assumptions this is only an indicator for stability. In appendix III the essence of the analysis is reproduced. The stability conditions are:

$$\frac{\gamma}{\Delta\theta} \leq \frac{k_y \cdot \Delta x}{2}$$
$$\frac{\gamma}{\Delta\theta} \leq \frac{k_x \cdot \Delta y}{2} \qquad (30)$$

in which k_x and k_y are a characteristic wave number in x- and y-direction respectively. It might seem surprising that a high resolution in geographical domain has a negative influence on the stability. This can be explained as follows. Eq. 26 indicates that the ratio of the diffraction-induced propagation term to the geographical propagation term should be smaller than a certain value. The diffraction term is a second-order term with derivatives in both spatial and directional domain. Therefore the magnitude of the aforementioned ratio is not only dependent on the resolution in θ-domain, but to the spatial resolution as well.

For the academic testcase as described in the next section (Δx = Δy = 10 m, ΔΘ = 4° and L = 40 m) the conditions yield:

$$\gamma \leq \frac{k_x \cdot \Delta y \cdot \Delta\theta}{2} = \frac{\frac{2\pi}{40} \cdot 10 \cdot 4}{2} = 3.14 \qquad (31)$$

It appeared that instability arose at a lower value for γ, approximately a hundredth of this analytical value (≈0.04). This is probably due to the assumptions that are made to carry out the analysis. Decreasing the directional resolution (i.e. increasing the interval ΔΘ) had a positive influence on the stability, which is in agreement with the stability condition.

METHOD OF THE STUDY

Mild-slope approach

The mild-slope approach is tested with the classical diffraction case of waves near a semi-infinite breakwater. It was not possible to obtain stable solutions. Although it seems conceptually possible to include a diffraction-induced turning rate based on second-order spatial derivative of the wave field the numerical techniques are not designed to compute these higher-order terms. In Appendix IV the attempts to make the model stable are mentioned.

Gradient approach

To test the gradient approach for diffraction three different cases are considered: (a) the classical Sommerfeld-solution for monochromatic, unidirectional waves near a semi-infinite breakwater (pure diffraction), (b) a situation with waves propagating over a navigation channel between two breakwaters and a fairly realistic harbour beyond a gap (combined refraction and diffraction) and (c) a realistic field case where long-crested and short-crested waves approach the Bay of Viano do Castelo (Portugal) which is protected from the ocean by a cape (combined refraction and diffraction).

The computations are made with as well as without the proposed formulation for diffraction to see the effect of the term. In the first testcase (the semi-infite breakwater) the value for the coefficient γ is varied to tune the model. Higher values for the coefficient γ gave better agreements with analytical solutions. However, due to numerical stability problems the value for the coefficient γ was limited to approximately 0.05. To compute the wave field in the cases (b) and (c) the tunable coefficient γ is chosen equal to 0.025. Although this value is considerably lower than the value that follows from the stability condition it is chosen since it is the highest possible value for which all the computations were stable.

For all tests computations are made for long-crested and for short-crested waves. The directional distribution is of the type $D(\Theta) = A_1 \cos^m(\Theta)$, where $m = 75$ for long-crested waves and $m = 10$ for short-crested waves. In Appendix I a description of the wave spectra is given. The corresponding directional spread is 6.6 degrees for long-crested waves and 17 degrees for short-crested waves. These values for the directional distribution are chosen to make a comparison with diffraction diagrams of Goda (1978) possible as will be explained later. The total one-sided width of the directional distribution is about 2.5 times the directional spread: 16.5 degrees for the long-crested waves and 42.5 degrees for the short-crested waves. The directional resolution is chosen such that the directional distribution is well resolved, which results in the following resolution: $\Delta\theta = 4°$ for simulated long-crested waves and $\Delta\theta = 10°$ for simulated short-crested waves. This corresponds

to eight spectral bins to represent the directional distribution.

The spatial resolution is chosen about a quarter of the wave length. The spatial grid is chosen identical to the bottom grid. This relatively high spatial resolution (high compared to the wave length) is chosen to minimize the numerical diffusion of the computation. This numerical diffusion is proportional to the spatial resolution (order $c_x\Delta x$). The numerical diffusion has a similar spreading influence on the wave field. Therefore the influence of the diffraction term can best be seen if the numerical diffusion is minimized. For the same reason a central difference scheme, which is less diffusive than an upwind scheme, is utilized to compute propagation in θ-direction. A second reason for choosing a high spatial resolution is the fact that diffraction plays a role on a scale of only a few wavelengths. The resolution should be sufficient to resolve the relevant spatial details (i.e. Δx and Δx should be chosen relatively low compared to the wavelength).

Academic tests

As mentioned before the classical Sommerfeld-solution for monochromatic, unidirectional waves near a semi-infinite breakwater (see Appendix V) is used to tune the gradient approach. Computations for this case are made with random short-crested waves (a young sea state represented by a JONSWAP spectrum and an old sea state represented by a Pierson-Moskowitz spectrum) and long-crested waves (a swell case represented by a Pierson-Moskowitz spectrum). The computations are also carried out with monochromatic waves.

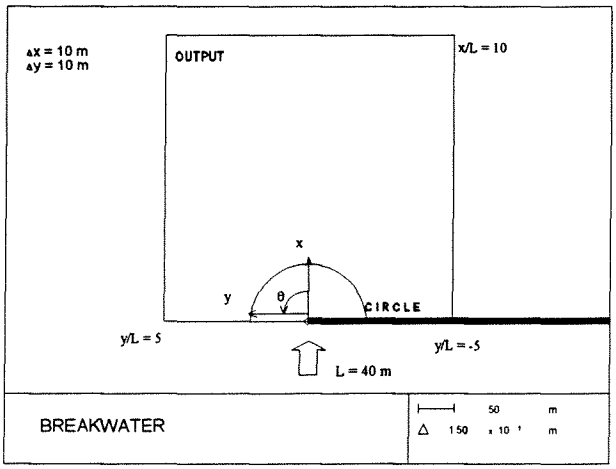

Figure 2. Computational area and output grid for a semi-infinite breakwater

The computational area is given in Fig. 2. The depth is 100 m and the mean wave length is 40 m with normal incidence. The breakwater is assumed to be fully absorbing. To avoid an erroneous influence of the boundary the breakwater is placed a few wave lengths away from the upstream boundary.

Computations for this academic test case with random, short-crested waves are compared with diffraction diagrams for a spectrum determined by Goda (1978). To give a spectral representation Goda splitted the spectrum in several directional components and determined the Sommerfeld-solution per component. Instead of a full discretization of the frequency spectrum a mean frequency is used. The diffraction diagrams are constructed by linear superposition of the

contributions of the components. Two diagrams are constructed by Goda, one for long-crested waves with a directional spread of 6.6 degrees (m = 75) and one for short-crested waves with a directional spread of 17 degrees (m = 10). The directional spreading function used in SWAN is similar to the one used by Goda, namely a directional distribution of the type $\cos^m(\theta)$.

In Fig. 3 the results of the computations (in terms of relative (significant) wave height H/H_i) with long-crested waves and a Pierson-Moskowitz spectrum are shown. The results shown in Fig. 3.a are obtained from computations without the proposed diffraction term. The directional spread of the waves is 6.6 degrees (m = 75). The pattern is spread out by introducing the diffraction term (with $\gamma = 0.025$) as shown in Fig. 3.b. The results of the computations obtained with the gradient approach show a deeper wave penetration in the shadow zone than the wave field computed without the proposed diffraction term. However, for both models the wave heights in the shadow zone are much lower than follows from the diagrams of Goda.

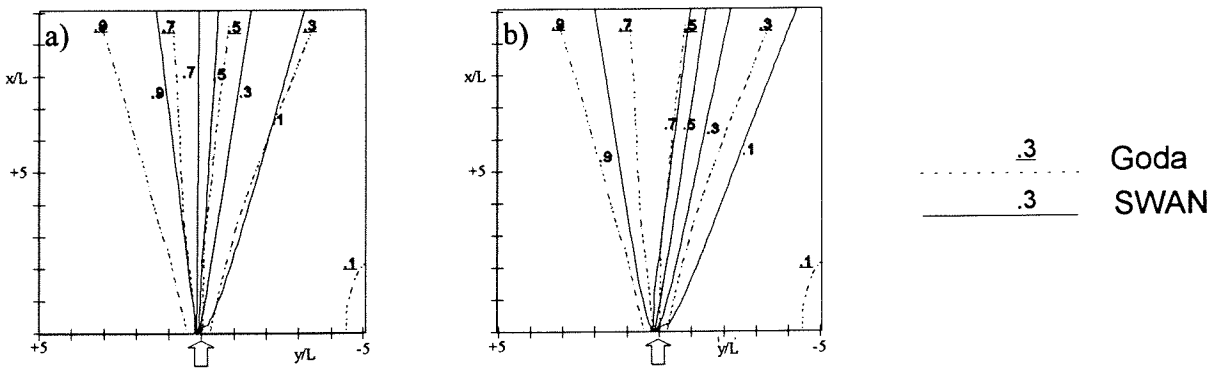

Figure 3. Comparison between computations and diffraction diagrams of Goda for long-crested waves behind a semi-infinite breakwater in terms of relative (significant) wave height H/H_i. Panel a) SWAN (no diffraction). Panel b) SWAN with diffraction-induced turning rate ($\gamma = 0.025$).

For short-crested waves a comparison is made between two frequency spectra (a JONSWAP spectrum and a Pierson-Moskowitz spectrum). The results are also compared with computations for monochromatic waves, which can be done by computing the spectrum for one single frequency. The difference between the results was small. This suggests that the frequency-wise irregularity is relatively unimportant in situations with diffraction. For this reason the two-dimensional spectrum in SWAN is replaced by a one-dimensional spectrum (i.e. monochromatic, directional random waves). In Fig. 4.a and 4.b the results of computations for short-crested waves (a Pierson-Moskowitz spectrum (a) and monochromatic waves (b)), without the proposed diffraction term are shown. The smoothing influence of short-crestedness is obvious from comparison with Fig. 3. The penetration of wave energy behind the obstacle is much higher than in the case of long-crested waves (Fig. 3). In Fig. 4.c and 4.d. the results of the computations with the diffraction term

are shown. Now the smoothing influence of the diffraction term is less important. The difference between the results obtained with the original formulation for the action balance equation (Fig. 4.a and 4.b) and those obtained with the gradient approach (Fig. 4.c and 4.d) is small. The iso-lines of the wave height in the shadow zone are hardly affected.

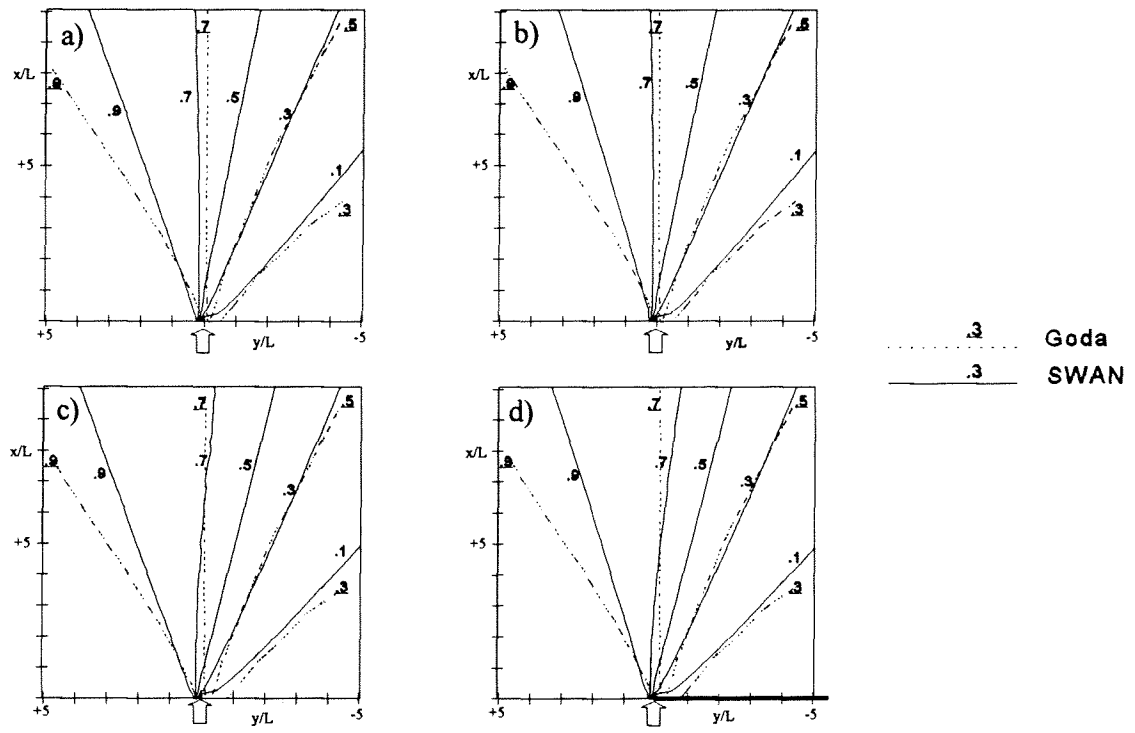

Figure 4. Comparison between computations and diffraction diagrams of Goda for short-crested waves behind a semi-infinite breakwater in terms of relative (significant) wave height H/H_i. Panels a,b) SWAN (no diffraction): a) Pierson-Moskowitz spectrum and b) monochromatic waves. Panels c,d) SWAN with diffraction-induced turning rate ($\gamma=0.025$): c) Pierson-Moskowitz spectrum and d) monochromatic waves.

A further comparison is made in Fig. 5, in which the results are shown of the computations (with increasing values for the coefficient γ) along a circle with radius of two wave lengths around the tip of the breakwater. Spectral estimates are obtained by linear superposition of monochromatic directional random waves, similarly to the construction of the diffraction diagrams of Goda. The solid line corresponds to this superposition of the classical Sommerfeld solution, the dashed line corresponds to the computations without the proposed diffraction term (thus the original formulation of the action balance equation in SWAN), the dotted line corresponds to the computations with the proposed diffraction coefficient γ equal to 0.01 and the dashed/dotted line to a diffraction coefficient γ equal to 0.05. In Fig. 5.a the results for long-crested, monochromatic waves are shown (directional spread is 6.6 degrees), whereas in Fig. 5.b the results for short-crested, monochromatic waves are given (directional spread is 17 degrees). The results confirm the

prior findings that the wave pattern is spread out by the diffraction term if there is no natural spread of the waves (i.e. long-crested waves) and that diffraction is relatively unimportant in the case of short-crested waves. In the former case the curve corresponding to the model with the diffraction term, is less steep. In the latter case the difference between the curves is rather small.

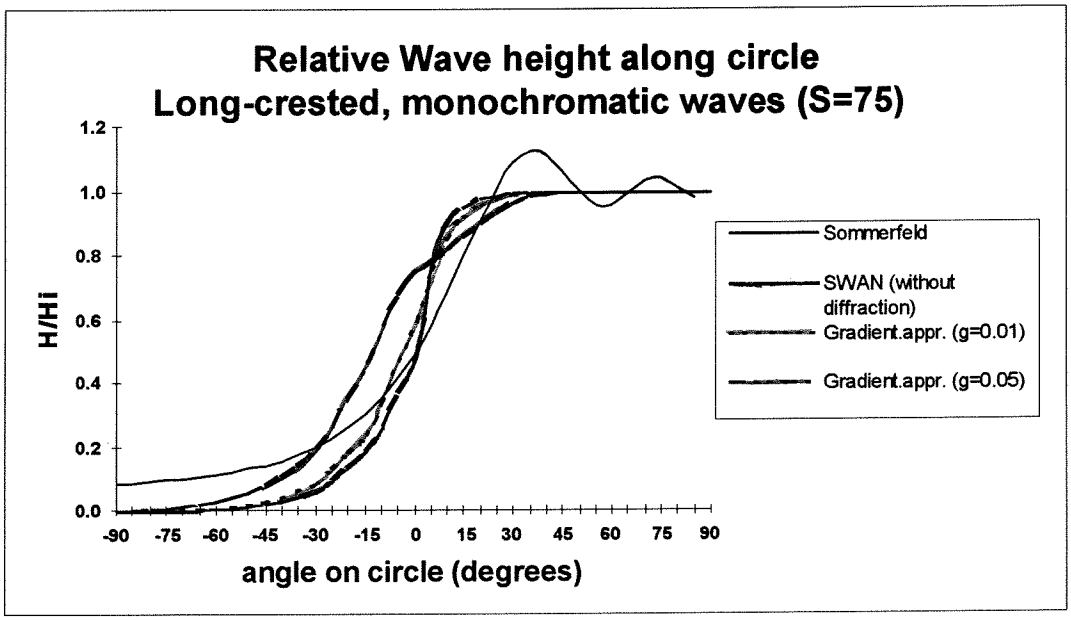

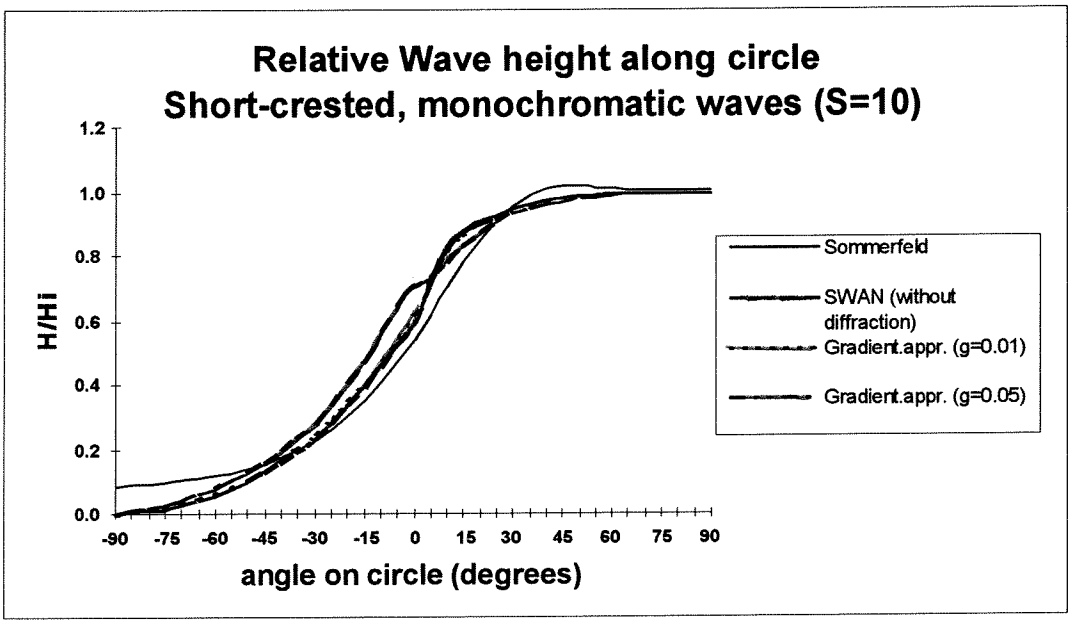

Figure 5. Results of the computations along the circle shown in Fig. 2. Panel a) Long-crested monochromatic waves (m = 75, which corresponds to a directional spread of 6.6 degrees). Panel b) Short-crested monochromatic waves (m = 10, which corresponds to a directional spread of 17 degrees).

In Fig. 6 the propagation direction for long-crested waves is given. Fig. 6.a corresponds to the SWAN-model without the proposed diffraction term and Fig. 6.b and 6.c to the model with the diffraction term ($\gamma = 0.01$ and $\gamma = 0.05$ respectively). In Fig. 7 the same is done for short-crested waves.

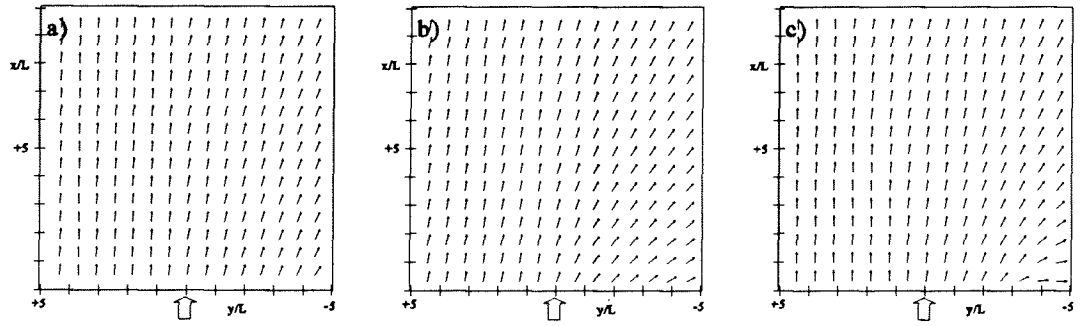

Figure 6. Propagation direction of long-crested waves (m = 75, which corresponds to a directional spread of 6.6 degrees). Panel a) SWAN (no diffraction). Panels b,c) SWAN with diffraction-induced turning rate ($\gamma = 0.01$ and $\gamma = 0.05$ respectively).

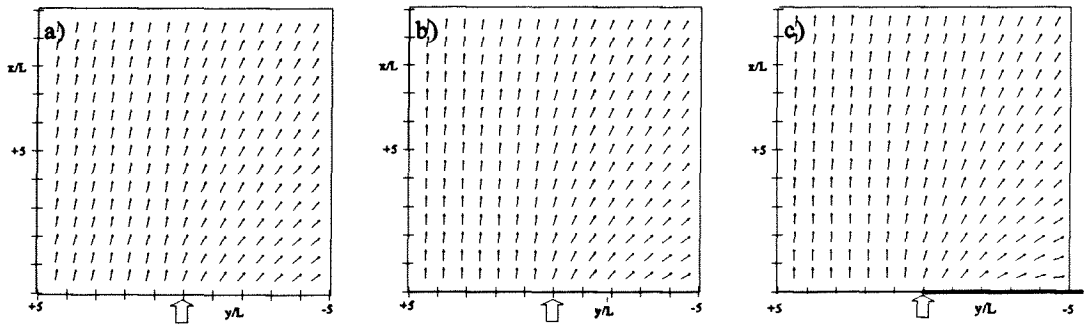

Figure 7. Propagation direction of short-crested waves (m = 10, which corresponds to a directional spread of 17 degrees). Panel a) SWAN (no diffraction). Panels b,c) SWAN with diffraction-induced turning rate ($\gamma = 0.01$ and $\gamma = 0.05$ respectively).

In Fig. 8 the propagation direction of the waves along the circle (as shown in Fig.2) at the lee-side of the breakwater is given. Immediately behind the breakwater the diffraction-term gives a considerable directional shift. The mean wave direction turns 60 degrees for long-crested waves and almost 50 degrees for short-crested waves.

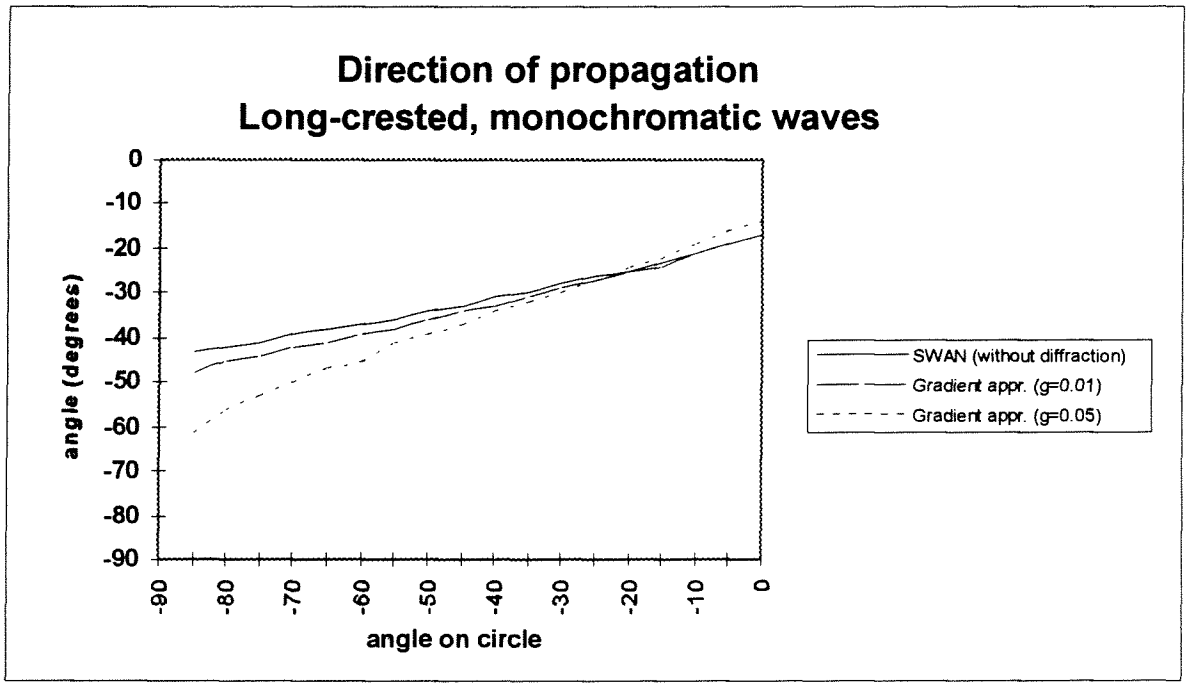

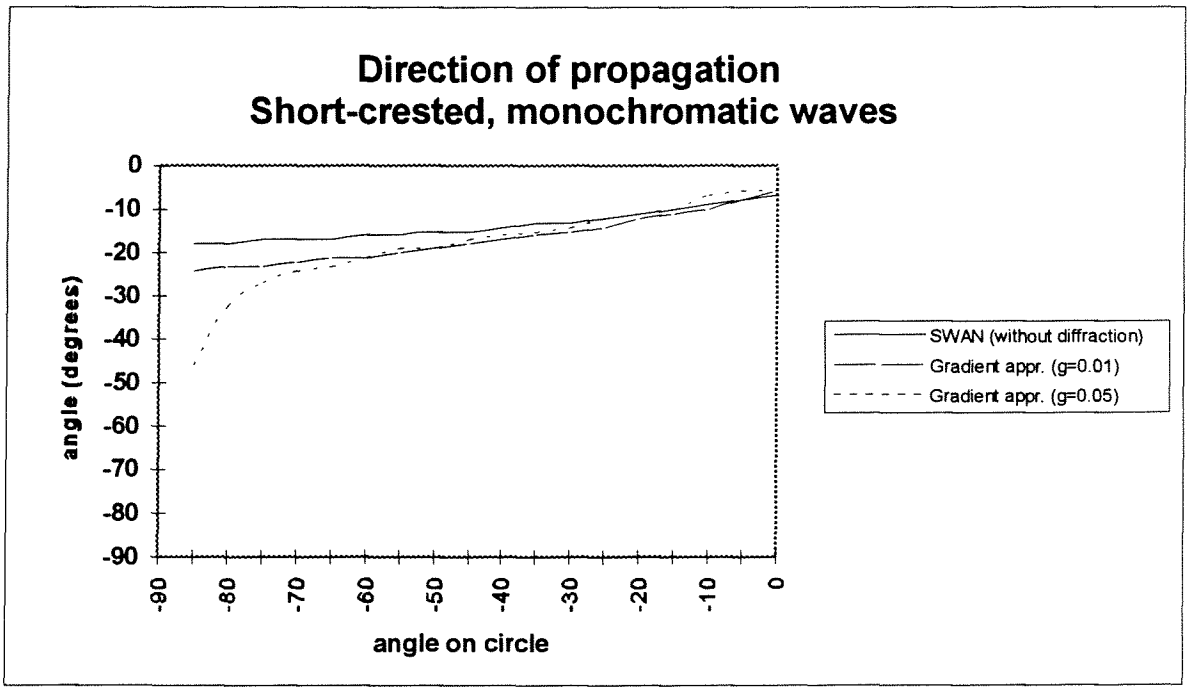

Figure 8. Direction of propagation at lee-side of the breakwater. Panel a) Long-crested waves and panel b) short-crested waves.

Harbour

The model is also applied to a fairly realistic harbour with a navigation channel. This harbour is used by Booij et al. (1992) to study the the significance of diffraction in relation to the significance of refraction. Two different types of models are used: the combined refraction-diffraction model PHAROS and the model HISWA, which is based on the action balance equation. Short-crestedness is simulated with a $\cos^4(\theta)$ distribution (which corresponds to a directional spread of 25 degrees). In the present study the results obtained with the model PHAROS are compared with the results obtained with SWAN (with as well as without the proposed diffraction term).

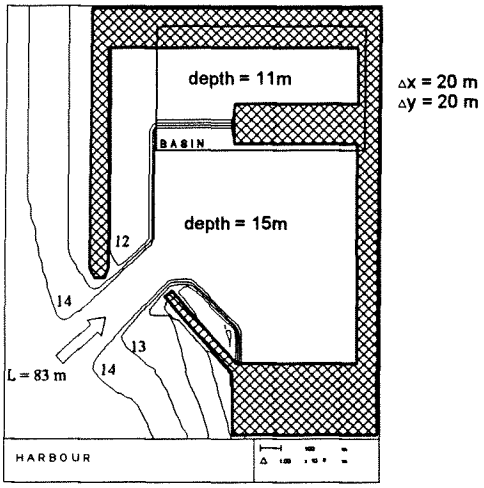

Figure 8. Bottom topography harbour with shallow basin.

In Fig. 8 the bottom topography is given for the harbour with the navigation channel. The channel originates in water of 15 m depth and the channel is maintained at that depth towards the deep water basin in the harbour at the same depth. Beyond the deep water basin, a shallow basin at 11 m depth is protected by a mole. The slope of the shoulders of the channel is 1:10 and the gap is 330 m wide (i.e. 4 wave lengths). For the purpose of this study the breakwaters are assumed to be fully absorbing. The incident significant wave height is 1 m and the mean wave length is 83 m. For economic reasons only monochromatic waves with a constant period of 10 s are considered. These values are the same as those used in the study of Booij et al. To make a comparison with the results obtained with PHAROS possible, the same spreading function (i.e.a $\cos^4(\theta)$ distribution) is used to simulate short-crestedness. The spatial grid resolution is chosen equal to the bottom grid: $\Delta x = \Delta y = 20$ m.

Computations are made with a mean wave direction along the channel axis. The shoulders of the channel refract the waves to the sides. In Fig. 9.a and 9.b the results are shown for long-crested waves ($m = 75$, which corresponds to a directional spread of 6.6 degrees) with as well as without the diffraction term respectively. There is a fairly deep penetration behind the left breakwater. The wave pattern is more or less spread in a finger pattern to the sides by the diffraction term. This **pattern** looks similar to the wave field computed with the model PHAROS (Fig. 10). Whereas the results obtained with the SWAN-model without diffraction show a concentration of action immediately behind the gap (Fig. 9.a), the results obtained with the gradient approach for diffraction (Fig. 9.b) and those obtained with the model PHAROS (Fig. 10) show wave pattern which is less concentrated immediately behind the gap. However, the computed wave heights

in the shallow basin are considerably higher than those computed with the model PHAROS.

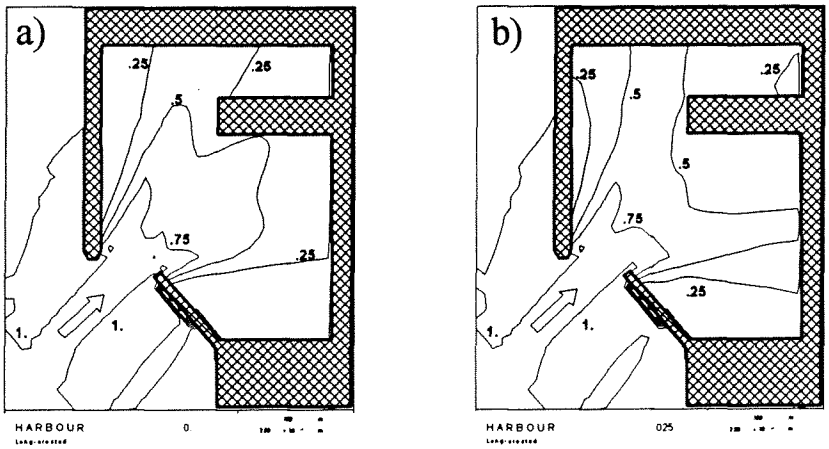

Figure 9 Penetration of long-crested waves in terms of relative (significant) wave height H/H_s. Panel a) SWAN (refraction only). Panel b) SWAN with gradient approach for diffraction ($\gamma=0.025$).

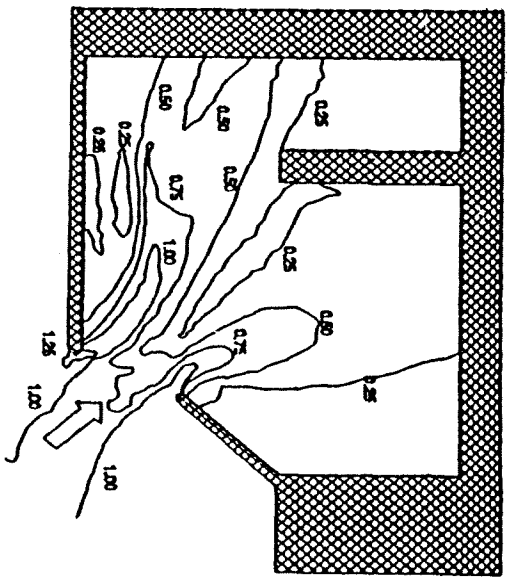

Figure 10. Penetration of long-crested waves obtained with the combined refraction-diffraction model PHAROS.

Introducing short-crestedness ($m=4$, which corresponds to a directional spread of 24.9 degrees) gives a deeper penetration of wave action behind the left breakwater (Fig. 11.a). In this case the influence of the diffraction term is hardly noticeable in the area where waves can penetrate with refraction (Fig. 11.c). However in the shallow basin the penetration of the waves is slightly higher for the computations with the diffraction term as can be seen in Fig. 11.b and 11.d, in which the wave penetration in the shallow basin is

shown. In the deep water basin there is a fairly good agreement between the wave heights computed with SWAN (with as well as without the gradient approach for diffraction) and the results obtained with the model PHAROS (Fig. 12). However, the wave penetration in the shallow basin computed with SWAN is considerably higher than the wave penetration computed with the model PHAROS.

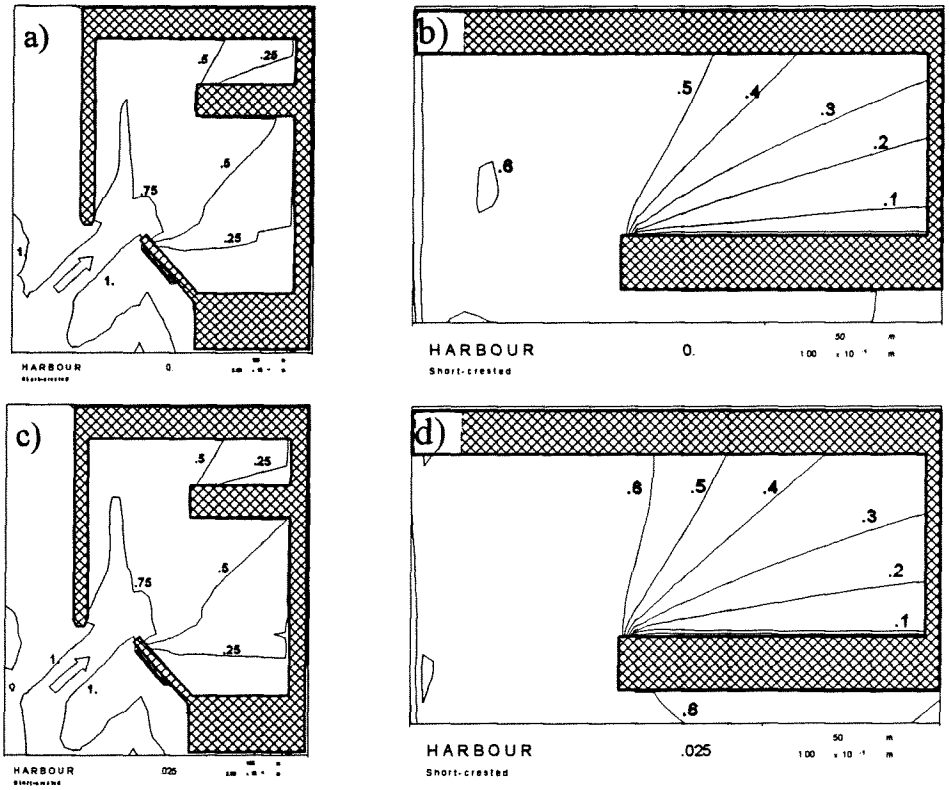

Figure 11. Penetration of short-crested waves in terms of relative (significant) wave height H/H_i. Panel a,b) Refraction model: total harbour (panel a) and shallow basin (panel b). Panel c,d) Refraction model with gradient approach for diffraction (γ=0.025): total harbour (c) and shallow basin (d).

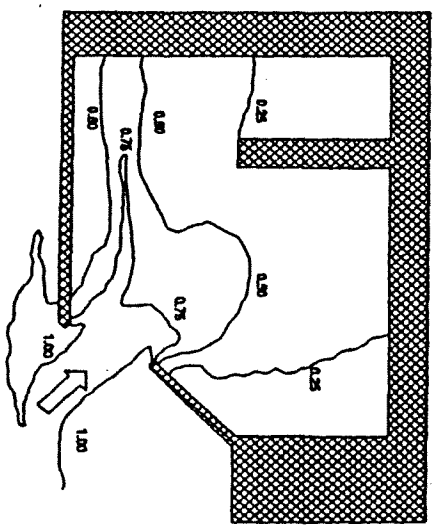

Figure 12. Penetration of short-crested waves computed with combined refraction-diffraction model PHAROS.

Viano do Castelo

The model is also applied to a realistic field case. It is a case where long-crested and short-crested waves approach the Bay of Viano do Castelo (Portugal) which is protected from the ocean by a cape. The bathymetry is given in Fig. 13. The wave period of the incident waves is 7.6 s and the significant wave height is 1 m. Although the resolution of the bottom grid in x-direction differed from the resolution in y-direction the spatial computational grid was chosen to be identical to the botttom grid. This is done to avoid that relevant spatial details in the bathymetry are 'lost'.

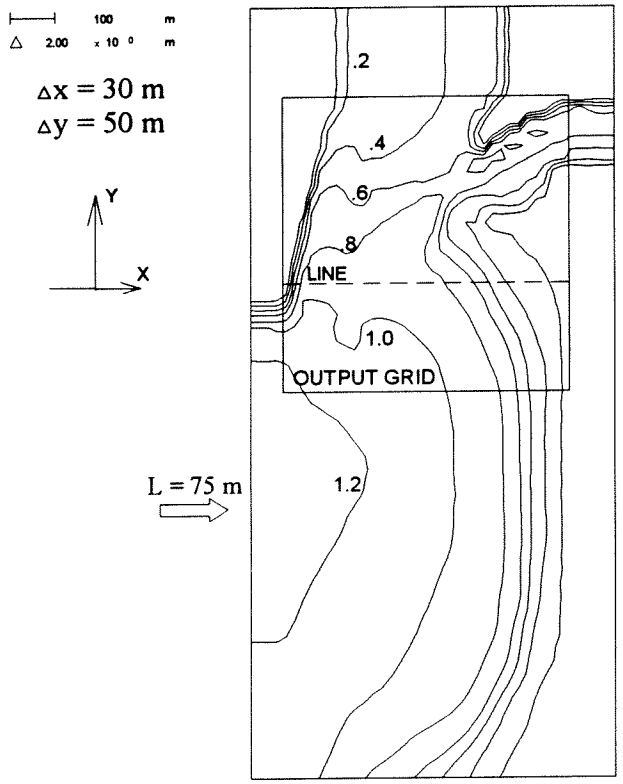

Figure 13. Computational area and output grid for Bay of Viano do Castelo

The results of the computations (in terms of the relative (significant) wave height in the centre of the bay) are shown in Fig. 14. For long-crested waves the diffraction term gives a smoothing of the wave field and a deeper penetration of wave energy, which is shown by the 0.1-isoline of the wave height (compare Fig. 14.a and 14.b). For short-crested waves the diffraction term has a minor effect. Only at the left-side of the centre the wave heights computed with the diffraction term are a bit higher. This indicates the relative unimportance of diffraction if there is a natural spread of the waves (short-crested waves).

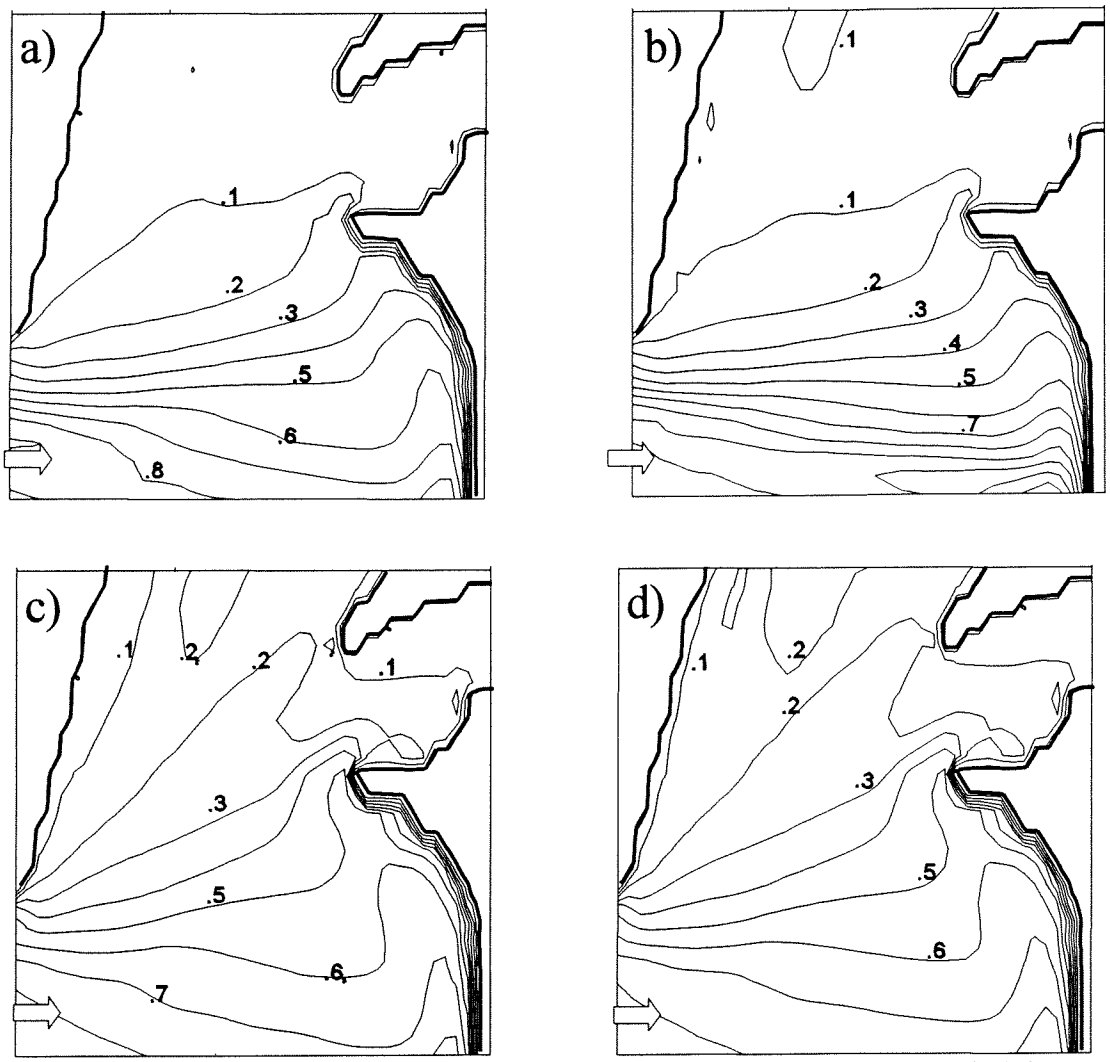

Figure 14. Wave penetration in Bay of Viano do Castelo. Panel a, c) SWAN (only refraction): longcrested waves (a) and short crested waves (c). Panel b, d) SWAN with gradient approach for diffraction: long-crested waves and short-crested waves (d)

The influence of the difraction term on the propagation direction of the waves is evaluated. In Fig. 15 the propagation direction of the waves along a section (denoted as LINE in Fig. 13) is shown. The incident wave direction is 0°. Therefore the direction shown in Figure 15 is the same as the change of direction from the incident waves. Refraction causes a directional shift of 25 to 90° as can be seen in the figure. In the case of long-crested waves the turning rate is slightly affected by the diffraction term. The change of propagation direction computed with the diffraction approach is lower than the change of direction computed without the diffraction term.

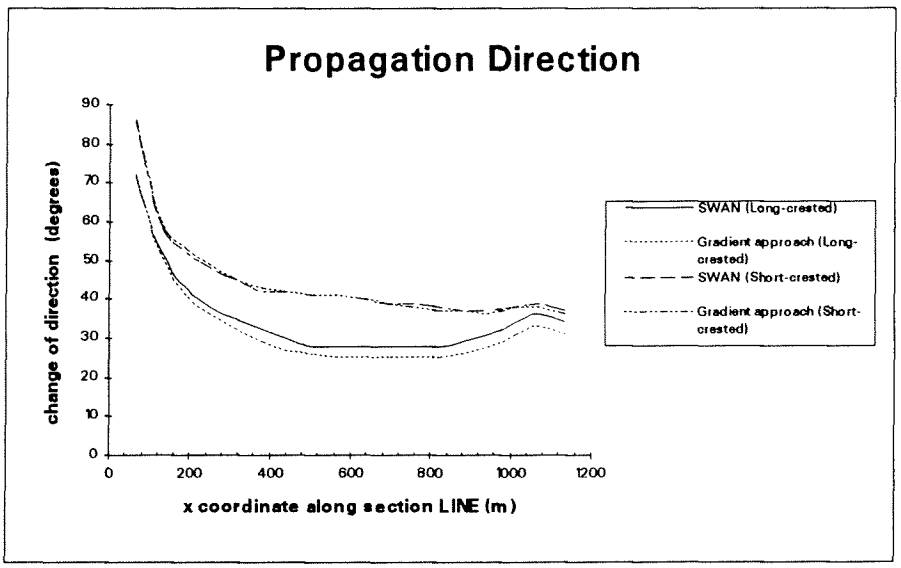

Figure 15. Propagation direction for long-crested and short-crested waves expressed as a change of direction from the incident wave direction.

CONCLUSIONS

The following conclusions were arrived at with respect to the inclusion of diffraction in a spectral wave model:

1. It seems conceptually possible to include diffraction in a spectral wave model by adding a diffraction-induced turning-rate to the refraction-induced turning rate of each individual wave component. Based on an ad-hoc reformulation of the mild-slope equation, this turning-rate can be estimated with a second-order derivative of the wave energy. However, the attempts to obtain stable solutions with the conventional numerical schemes of the spectral wave model SWAN failed. The numerical techniques in SWAN are specifically designed to solve the first-order propagation terms efficiently. The solution of higher-order terms requires a drastic change of the computational part of the model, which will result in a loss of efficiency of the model.
2. A second approach for diffraction is to include a turning-rate, based on the first-order gradient of the wave energy density. The purpose of this term is not to produce an accurate representation of diffraction but to spatially smooth the wave field in areas with strong spatial gradients. For long-crested waves this term caused a spreading of the wave field.
3. In areas with considerable wave motion even in absence of diffraction, the effect of diffraction is small. In these regions the results obtained from a refraction model (i.e. without diffraction) seem to give a reliable estimate of the wave field. In other cases, such as long-crested waves immediately behind breakwaters, diffraction is dominant. In such situations the gradient approach causes a deeper penetration of wave energy.
4. For most practical applications the inclusion of short-crestedness in a numerical model is more important than the inclusion of diffraction. For example in harbours with a varying depth a refraction model (without diffraction but with the inclusion of short-crestedness) will give a more realistic estimate of the wave field than a refraction-diffraction model in which short-crestedness is not accounted for. Moreover, the computing power required for a refraction model is considerably less than for a refraction-diffraction model.
5. Computations for a diffraction situation are made, with both a fully spectral description of the wave field and a one-dimensional spectrum, in which the frequency spectrum is replaced by one single discrete frequency. The difference between the results is small, which indicates that the frequency-wise irregularity of the wave spectra is relative unimportant in case of diffraction.

Recommendations

The concept of a diffraction-induced turning rate derived from the second-order derivatives of the wave field seems to be soundly based. From scientific point of view it is recommended to implement the mild-slope approach in a spectral model, of which the numerical techniques allow higher-order derivatives.

For practical applications it is probably better to simulate diffraction only locally, in areas where diffraction is dominant. This can possibly be done with a nested diffraction-refraction model, which is used in areas with strong spatial gradients only. In the other grid points the wave field is computed with the 'main model'.

ACKNOWLEDGEMENTS

This report is written as a masters thesis at the Delft University of Technology, Faculty of Civil Engineering. I would like to thank all those who supported and assisted me during this study.

Most of all I wish to express my gratitude to dr. L.H. Holthuijsen and dr. N. Booij for critically reading the manuscript and for their guidance during the entire project. I wish to thank prof. J.A. Battjes for his valuable comments and his stimulating support. Ir. R. Ris is acknowledged for his assistance with the numerical part of the study.

REFERENCES

Abbott, M.B. and Basco, D.R., 1989. *Computational Fluid Dynamics*, John Wiley & Sons, Inc., New York.

Battjes, J.A., 1968. 'Refraction of Water Waves'. *J. of the Waterways and Harbors Division*, ASCE, Vol. 94, No. WW4. Proc. Paper 6206, pp 437-451.

Berkhoff, J.C.W., 1972. 'Computation of Combined Refraction - Diffraction'. *Proc. 13th Int. Conf. Coastal Eng.*, Vancouver, Canada, ASCE, pp 471-490.

Biesel, F., 1972. 'Réfraction de la houle avec diffraction modérée'. *Proc. 13th Int. Conf. Coastal Eng.*, Vancouver, Canada, ASCE, pp 491-501.

Booij, N., 1981, *Gravity waves on water with non-uniform depth and current*. Rep. No. 81-1, Delft University of Technology.

Booij, N., Holthuijsen, L.H. and de Lange, P.H.M., 1992. 'The penetration of short-crested waves through a gab'. *Proc. 23th Int. Conf. Coastal Eng.*, pp 1044-1052.

Bretherton, F.P. and C.J.R. Garrett, 1968. 'Wave trains in inhomogeneous moving media'. *Proc.Roy.Soc.London*, A, 302, pp.529-554.

Dingemans, M.W., 1985. *Surface wave propagation over an uneven bottom. Evaluation of two-dimensional horizontal wave propagation models*. Report W301 part 5, Delft Hydraulics Laboratory.

Gao, Q., Radder, A.C., Booij., N., 1993. *A numerical Wave Model for the Refraction and Diffraction of irregular waves. Description of the Wave Model CREON*. Report 5-93. Delft University of Technology.

Goda Y. et al., 1978. 'Diffraction Diagrams for Directional Random Waves' *J. of Coastal Eng.*, Vol. 1, pp 628-650.

Holthuijsen, L.H., 1980. *Methoden voor golfvoorspelling*. Technische Adviescommissie voor de Waterkeringen, 's-Gravenhage.

Holthuijsen, L.H., N. Booij, 1986. 'A grid model for shallow water waves'. *Proc. 20th Int. Conf. Coastal Eng.*, Taipei, pp 261-270.

Holthuijsen, L.H., N. Booij and R.C. Ris, 1993. 'A spectral wave model for the coastal zone'. *Proc. 2nd Int. Symposium on Ocean Wave Measurement and Analysis*, New Orleans, pp 630-641.

Kinsman, B., 1965. *Wind waves, Their Generation and Propagation on the Ocean Surface*, Prentice Hall, Inc., Englewood Cliffs.

Kirby, J.T. and Dalrymple, R.A., 1983. A parabolic Equation for the combined refraction-diffraction of Stokes waves by mildly varying Topography. *J. of Fluid Mech.* 136, 453-466.

Mei, C.C., 1983. *The applied Dynamics of Ocean Surface Waves*. Wiley, New York.

Panchang, V.G. Ge, W., Pearce, B.R. and Briggs, M.J., 1990. Numerical simulation of irregular wave propagation over a shoal. *J. of Waterway, Port, Coastal and Ocean Eng.*, ASCE 116(3), pp. 324-340.

Peregrine, D.H., 1967. Long waves on a beach. *J. of Fluid Mech.*, 27(4), pp. 815-827.

Phillips, O.M., 1969. *The Dynamics of the Upper Ocean*. Cambridge University Press.

Radder, A.C., 1979. On the Parabolic Equation Method for Water-wave Propagation. J. of Fluid Mech. 136, 435-452.

Resio, D.T., 1988. 'A Steady-State Wave Model for Coastal Applications'. *Proc. 21th Int. Conf. Coastal Eng.*, pp 929-940.

Ris, R.C., L.H. Holthuijsen and N. Booij, 1994. 'A Spectral Model for Waves in the Near Shore Zone'. *Proc. 24th Int. Conf. Coastal Eng.*, Kobe, pp 68-78.

Ris, R.C., L.H. Holthuijsen and N. Booij, 1995. *SWAN Cycle 1, User Manual*. Delft University of Technology, Department of Civil Eng.

Rivero, F.J., -Arcilla, A.S., 1993. 'Propagation of Linear Gravity Waves over slowly varying Depth and Currents'. *Proc. of the Int.Conf. WAVES '93*, New Orleans, USA, ASCE, pp 518 - 532.

Sommerfeld, A., 1896. 'Mathematische Theorie der Diffraction'. *Mathematische Annals*, Vol. 47, pp 317-374.

Tolman, H.L., 1991. 'A third generation model for wind waves on slowly varying, unsteady, and inhomogeneous depths and currents', *J. of Phys. Oceanography.*, 21 (6), pp 782-797.

Vincent, C.L. and Briggs, M.J., 1989. Refraction-diffraction of irregular waves over a mound., *J. of Waterway, Port, Coastal and Ocean Eng.*, ASCE 115(2), pp. 269-284.

WAMDI group (Hasselman et al.), 1988. 'The WAM model - a third generation ocean wave prediction model', *J. of Phys. Oceanography*, 18, pp. 1775-1810.

WMO, 1976. *Handbook on Wave Analysis and Forecasting*. Geneva: World Meteorological Organization.

NOTATION

Symbol	Definition	Dimension
A	Amplitude in velocity potential	L^2T^{-1}
A_1	Coefficient in spreading function	-
a	Wave amplitude	L
c	Phase speed; the speed of propagation of a wave	LT^{-1}
c_g	Group velocity; the propagation velocity of energy, underlining denotes vector representation	LT^{-1}
c_x, c_y	Propagation velocity in x and y-direction	LT^{-1}
c_σ	Propagation velocity in σ-direction	T^{-2}
c_θ	Propagation velocity in Θ-direction	T^{-1}
d	Water depth	L
D_f	Directional spreading function	-
E	Spectral wave energy density	$MT^{-2}Hz^{-1}$
f	Frequency	T^{-1}
g	Gravitational acceleration	LT^{-2}
H	Wave height	L
k	Wave number, underlining denotes vector representation	L^{-1}
K	Wave number derived from the mild-slope equation	L^{-1}
L	Wave length	L
m	Coordinate along wave crest	L
m	Coefficient in spreading function	-
N	Wave action density in spectral space	$MT^{-1}Hz^{-1}$
$\underline{n}$	Unit vector	-
P	Pressure	$LM^{-1}T^{-2}$
S	Source function	T^{-4}
S	Bottom slope	-
s	Coordinate in propagation direction	L
T	Wave period	T
t	Unit of time	T
$\underline{U}$	Current velocity	LT^{-1}
x, y	Horizontal space coordinates, underlining denotes vector representation	L
z	Vertical space coordinate	L
α	Parameter in PM- and JONSWAP-spectrum	-
α, ß	Coefficients in SWAN to determine numerical scheme	-
γ	Peak enhancement factor	-
γ	Tunable coefficient (gradient approach)	-
Δx, Δy	Resolution in x, y-domain	L
ΔΘ	Resolution in Θ-domain	-
Δσ	Resolution in σ-domain	T^{-1}
ε	Spectrum width parameter	-
η	Elevation of the free surface	L
θ	Direction of wave propagation	-
ρ	Density of water	ML^{-3}
ρ	Amplification factor	-
σ	Relative frequency	T^{-1}
σ_a, σ_b	Coefficient for width of peak enhancement factor (left side and right side)	-
ϕ	Velocity potential	LT^{-1}
ψ	Phase function	-
ω	Angular frequency	T^{-1}
∇	Horizontal gradient operator; subscripts denote partial differentiation	L^{-1}

APPENDICES

Appendix I : Physical Background

Appendix II : Numerical Background

Appendix III : Stability Analysis

Appendix IV : Attempts to make the model stable

Appendix V : Sommerfeld-solution

APPENDIX I: PHYSICAL BACKGROUND

I.1 Wave Fundamentals and Classification of Waves

Many types of waves involving different physical factors exist in the ocean. It is important to distinguish between the various types of water waves that may be generated and propagated. Waves can be classified by the wave period T (the time for a wave to travel a distance of one wavelength) or according to the restoring force. Figure I.1 is an illustration of classification by period or frequency given by Kinsman (1965).

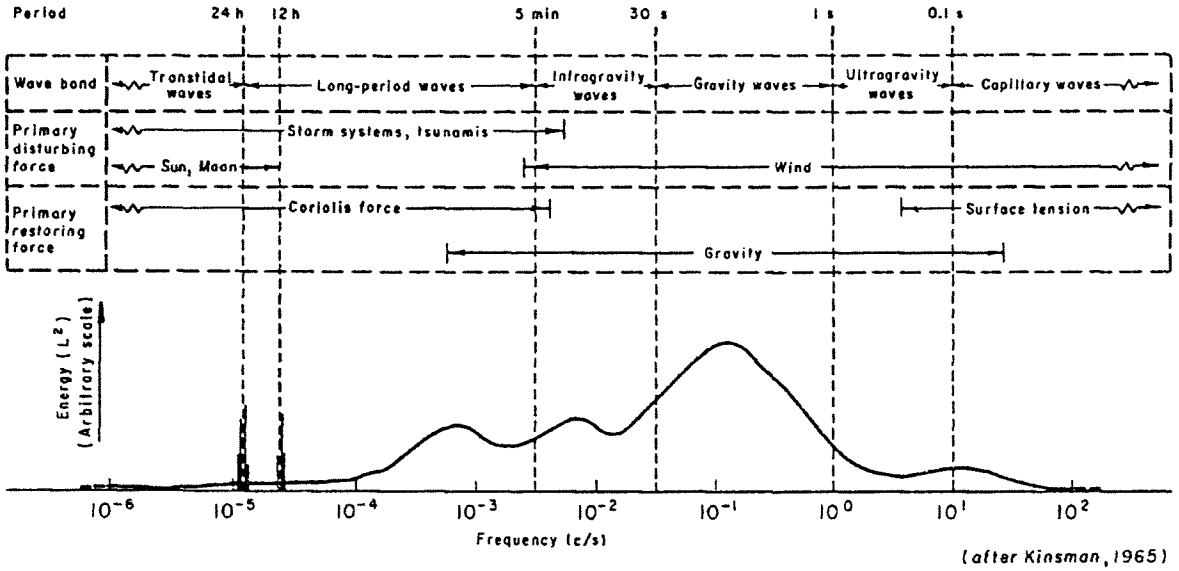

Figure I.1 Approximate distribution of ocean surface wave energy, with the classification of surface waves by the wave band, primary disturbing force, and primary restoring force.

The figure shows the relative amount of energy contained in ocean waves having a particular frequency. The waves referred to as gravity waves (or better surface gravity waves), which have periods from 1 to 25 seconds, are of interest for this thesis. These waves are referred to as gravity waves since gravity is the main restoring force. As in the elementary problem of a spring-mass system, all waves must be associated with some kind of restoring force that attempts to return the fluid in its equilibrium position. The figure shows that a large amount of energy is associated with waves classified as gravity waves; hence gravity waves are extremely important in dealing with the design of coastal and offshore structures.

Gravity waves can be further separated into two states:

(a) Wind sea, when the waves are under the influence of wind in a generating area;

(b) Swell, when the waves move out of the generating area and are no longer subjected to significant wind action.

Windsea is usually made up of steeper waves with shorter periods and lengths, and the surface appears much more disturbed than for swell. Swell behaves much like a free wave (i.e. free from the disturbing force that caused it), while windsea consists to some extent of forced waves (i.e. waves on which the disturbing force is applied continuously). As ocean waves are complex some simplifications are made in describing them, dependent on the theory used.

The following assumptions are commonly made in describing the gravity waves:

With regard to the external field of force:

- The gravity field is homogeneous; therefore g is a constant.
- The rotation of the earth (Coriolis effect) can be neglected.

With regard to the water:

- The fluid is ideal or inviscid.
- The fluid is homogeneous and incompressible; therefore the density ρ is a constant.

With regard to the motion:

- The motion is irrotational, which leads to a potential formulation.

With regard to the boundaries:

- Surface tension can be neglected.
- The bed is a fixed, impermeable boundary, which implies that the vertical velocity at the bed zero.

I.2. Mathematical Formulations

Before starting a mathematical description of the wave propagation it is important to give a definition of the coordinate-system used. The z-axis is positive upwards, with the still water level as the horizontal datum level (see Figure I.2). The surface elevation is referred to as a(x,y,t).

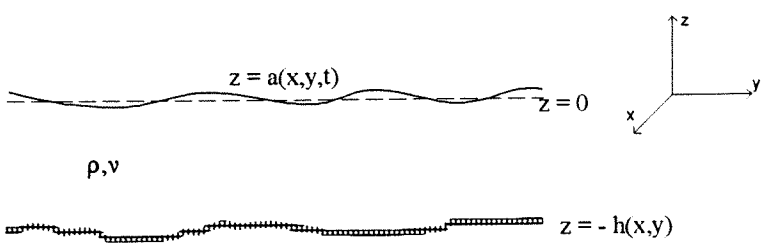

Figure I.2 Definition sketch

Governing Equations

As said before, in describing gravity waves the variation of water density is insignificant over the temporal and spatial scales of (engineering) interest and can be neglected. Moreover, since the motion is assumed to be irrotational, harmonic in time and the fluid to be ideal (i.e. the viscosity equals zero) the fundamental conservation laws are adequately described by the following equations (e.g. Mei, 1983):

- conservation of mass (Equation of Laplace)

$$\nabla^2\phi=0 \qquad (I.1)$$

- conservation of momentum (Equation of Bernoulli)

$$\frac{\partial\phi}{\partial t}+\frac{1}{2}(\nabla\phi\cdot\nabla\phi)+\frac{P}{\rho}+gz=0 \qquad (I.2)$$

The velocity potential can be written as

$$\phi=A(x,y,z)e^{-i\psi(x,y,z)t} \qquad (I.3)$$

Since in shallow water of variable depth d(x,y) the wave number k will no longer be constant, the amplitude A and the phase function ψ are not only dependent on x and y but on z as well.

Boundary Conditions

The velocity potential must fulfill the above mentioned Laplace Equation (Eq. I.1) and the boundary condition at the free surface:

$$\phi_{tt}+g\phi_z=0 \qquad (I.4)$$

and at the impermeable bed (z = -d)

$$\nabla\phi\cdot\underline{n}=0 \qquad (I.5)$$

in which $\underline{n}$ is the unit vector normal to the bottom. As Eqs. I.1, I.4 en I.5 must hold for all t, they can be rewritten as

$$\nabla^2A-A(\nabla\psi)^2=0 \qquad (I.6)$$

and

$$2\nabla A\cdot\nabla\psi+A\nabla^2\psi=0 \qquad (I.7)$$

At z = 0:

$$g\frac{\partial A}{\partial z}-\omega^2A=0 \qquad (I.8)$$

and

$$\frac{\partial\psi}{\partial z}=0 \qquad (I.9)$$

At z = -d:

$$\nabla A\cdot\underline{n}=0 \qquad (I.10)$$

and

$$\nabla\psi\cdot\underline{n}=0 \qquad (I.11)$$

Propagation Properties

The relative difference of $|\nabla \psi|$ near the surface and the bottom is of order S^2 (in which S is the bottom slope in the direction of propagation) and therefore negligible for practical purposes (Battjes, 1968). Thus, the phase function ψ can be considered independent of z.

Assuming that the vertical variation of A is locally the same over bottoms of small slope as it is over horizontal bottoms, gives the amplitude A

$$A(x,y,z)=\frac{A(x,y,z)}{A(x,y,0)}A(x,y,0) \qquad (I.12)$$

The variable z can be separated from x en y by replacing the quotient in Eq. I.12 by f(z) and substituting into Eq.I.6 yields

$$\frac{f_{zz}}{f}=(grad\ \psi)^2-\frac{A_{xx}(x,y,o)+A_{yy}(x,y,0)}{A(x,y,0)} \qquad (I.13)$$

Since the left hand member is a function of z and the right hand side member is a function of x en y only, both must be constant, denoted as k^2. Combination of Eq. I.10 and I.13 yields

$$f(z)=\frac{\cosh\ k(d+z)}{\cosh\ kd} \qquad (I.14)$$

Let a(x,y) be the local wave amplitude. The condition of constant pressure at the free surface gives

$$a(x,y)=\frac{\omega}{g}A(x,y,0) \qquad (I.15)$$

Combination of Eq. I.14 and I.15

$$A(x,y,z)=\frac{ga(x,y)}{\omega}\frac{\cosh\ k(d+z)}{\cosh\ kd} \qquad (I.16)$$

and substitution into Eq. I.9 gives

$$\omega^2=gk\ \tanh\ kd \qquad (I.17)$$

which is called the dispersion relation.

The phase speed is given by

$$c=\frac{\omega}{k}=(\frac{g}{k}\tanh\ kh)^{1/2} \qquad (I.18)$$

To describe the effects of refraction and diffraction Berkhoff (1976) derived the mild-slope equation:

$$\nabla c_g c(\nabla\phi_0)+\omega^2\frac{c_g}{c}\phi_0=0 \qquad (I.19)$$

Substitution of $\phi_0=a(x,y)e^{\psi(x,y)}$, with

- a(x,y) = an amplitude function
- ψ(x,y) = a phase function

into the mild-slope equation gives an equation with a real and an imaginary part. Equating the real part to zero gives an equation for the phase function including a gradient of the amplitude function:

$$(\nabla\psi)^2=k^2+\frac{\nabla(cc_g\nabla a)}{cc_g a} \qquad (I.20)$$

Equating the imaginary part to zero gives an equation for the amplitude function which contains derivatives of the phase function. The latter equation is equivalent to the wave energy balance. With these two equations solutions can be obtained for simple harmonic linear water waves.

I.3. Wave Spectra

The following standard frequency spectra are used in the model SWAN, a Pierson-Moskowitz or a JONSWAP spectrum. The amount of incoming energy density and the shape of these spectra are determined by a significant wave height H_s, a peak wave period T_{peak}, a mean wave direction θ and a directional distribution, denoted with $\cos^m(\theta)$.

- **The Pierson-Moskowitz-spectrum**

This spectrum is based on wave measurements recorded on board British weather ships (1955-1960). The spectrum is restricted to fully developed sea. It is described by the following formula:

$$E(f)=\alpha g^2(2\pi)^{-4}f^{-5}\exp(-\frac{5}{4}(\frac{f}{f_p})^{-4}) \qquad (I.21)$$

in which E(f) is the energy density, f the frequency, f_p the peak frequency, g the acceleration of gravity and α a dimensionless parameter equal to 0.0081.

- **The JONSWAP-spectrum**

This spectrum is based on the PM-spectrum but is adapted with the so-called "peak enhancement" factor for a growing sea:

$$E(f)=\alpha g^2(2\pi)^{-4}f^{-5}\exp(-\frac{5}{4}(\frac{f}{f_p})^{-4})\gamma^{\exp(\frac{-(f-f_p)^2}{2\sigma^2 f_p^2})} \qquad (I.22)$$

where σ_a = 0,07 for $f \le f_p$

σ_b = 0,09 for $f > f_p$

The coefficient α is dependent on the peak enhancement parameter, the significant wave height and the peak frequency:

$$\alpha=\frac{H_s^2\sigma_p^4}{16g^2(0.065\gamma^{0.803}+0.135)} \quad for \quad 1<\gamma<10 \qquad (I.23)$$

- **Directional Distribution**

Wave spectra are not only a function of the frequency but of the direction as well. Use is made of a directional spreading function, which is defined a follows:

$$D_f(\theta)=\frac{E(f,\theta)}{E(f)}, \quad whereas \int_0^{2\pi} D_f(\theta)d\theta=1 \qquad (I.24)$$

The directional width of the spectrum (directional spread DSPR) is defined as:

$$[DSPR]^2=\int_{-\pi/2}^{\pi/2}(2\sin(\theta-\bar{\theta}/2))^2 D(\theta)d\theta \qquad (I.25)$$

The spreading functions can be based on experiments, but it is more common to use mathematical formulations for the spreading functions. The following formulation is used SWAN:

$$D_f(\theta)=A_1\cos^m(\theta) \quad for \quad |\theta|<\pi/2$$
$$D_f(\theta)=0 \quad for \quad |\theta|\ge\pi/2 \qquad (I.26)$$

The value for m must be provided by the user. The coefficient m is related to the directional width of the spectrum (DSPR) as follows:

[m]	DSPR (in °)
1.	37.5
2.	31.5
3.	27.6
4.	24.9
5.	22.9
10.	17.1
75.	6.6
100.	5.7

APPENDIX II: NUMERICAL BACKGROUND

II.1. Introduction

The traditional coastal wave models were based on linear wave ray theory, which gives a general understanding of the wave propagation phenomenon. These models compute wave transformations due to bottom refraction by tracing wave rays from deep water to the shore and assuming that the energy flux is conserved between two adjacent rays. This technique often results in chaotic wave ray patterns, which are difficult to interpret. This can be avoided by using an Eulerian formulation (i.e. refraction computations on a regular grid). Such a model ensures a smooth representation of the wave pattern, because of the inherent spatial smoothing. Moreover, the nonlinear wave generation or dissipation can be represented efficiently.
In the present study the model SWAN (**S**imulation of **WA**ves in **N**earshore areas) is used to implement the diffraction-induced turning rate in a numerical refraction model. SWAN is a third generation fully spectral model based on the spectral action balance equation with sources and sinks (Holthuijsen et al., 1993; Ris et al., 1994).

II.2. Action Balance Equations

The principal prognostic quantity in the phase-averaged description of the wave field is the two-dimensional spectral distribution function of wave energy or action. Wave action is wave energy divided by the intrinsic frequency. The advantage of using wave action rather than wave energy is the fact thatwave action is conserved in case of wave-current interactions (Bretherton and Garrett, 1968). In the absence of currents the action balance equation reduces to the energy balance equation. In its general formulation the action balance equation can be written as:

$$\frac{\partial}{\partial t}N(\sigma,\theta)+\nabla_{x,y}[\underline{c}\ N(\sigma,\theta)]+\frac{\partial}{\partial\sigma}[c_\sigma N(\sigma,\theta)]+\frac{\partial}{\partial\theta}[c_\theta N(\sigma,\theta)]=\frac{S(\sigma,\theta)}{\sigma} \qquad (II.1)$$

in which $N(\sigma,\theta)$ is the action density of the waves, as a function of the intrinsic frequency σ and the spectral wave direction θ. The first term in the left-hand side of Eq. II.1 represents the rate of change of action in time. The second and third term represent propagation of action density in geographical space. The fourth term represents the shift of intrinsic frequency (due to variations in depths and currents) and the fifth term represents propagation of action density in the directional domain (refraction). The term $S(\sigma,\theta)$ in the right-hand side of Eq. II.1 represents the different source terms (formulated in terms of wave energy).

Numerical Schemes

The numerical technique for the propagation through the spectral space is somewhat similar to the techniques that has been used in parabolic models. In these models a forward marching method is used in which the computations progress line-by-line in one principal direction. For stability reasons the propagation is therefore limited to a certain directional sector to either side of the direction of the x-axis. In practice this corresponds to about 60°. This restriction excludes the effects of extreme refraction, reflections or cross seas. Moreover the computational grid has to be oriented in the mean wave direction which is operationally inconvenient. To overcome these problems the SWAN model has been developed, which is fully discrete spectral (over the total range of wave frequencies and directions). In SWAN a so called four-sweep technique is used. The directional domain is divided into four quadrants. First the state in grid point (x_i,y_i) is determined from two up-wave points (x_{i-1},y_i) and (x_i,y_{i-1}) (see Figure II.1).

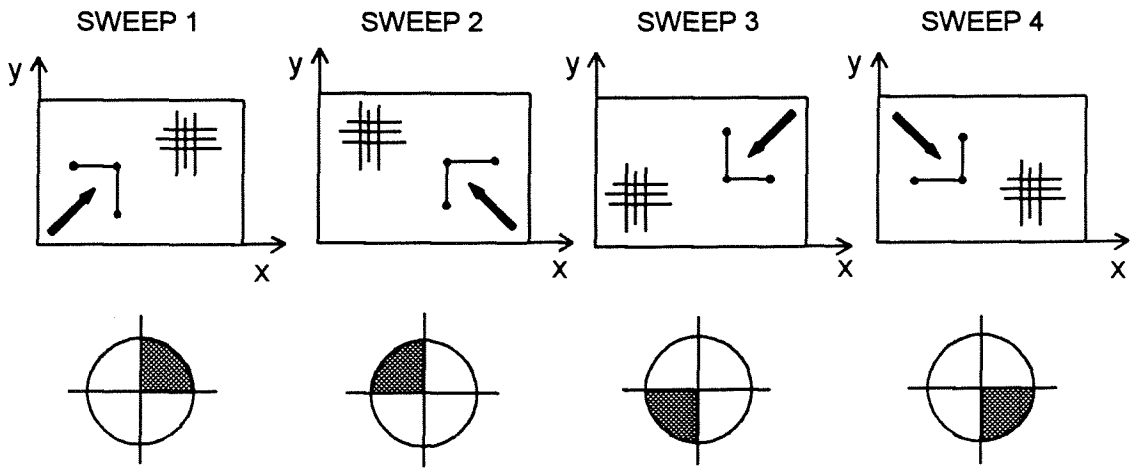

Figure II.1 Numerical Schemes for wave propagation in SWAN.

This stencil covers the propagation of action density within a sector of 0°-90°. A first order upwind scheme is used to ensure unconditionally stable integration. Now the stencil is rotated over 90° and the same procedure is repeated for waves that enter within the sector 90°-180°. The stencil is rotated twice more to cover all four quadrants. The influence of refraction (and therefore waves possibly shifting from one quadrant to another) is taken into account by repeating the computations with converging results.

The iterative procedure is repeated until the following convergency conditions are fulfilled:

a) Relative or absolute change in significant wave height less than a user-defined limit, and

b) Relative or absolute change in mean wave period less than a user-defined limit, and

c) conditions a) and b) are fulfilled in more than a user-defined percentage (e.g. 97%) of all wet grid points.

By means of a numerical coefficient α the user can choose between an implicit central difference scheme ($\alpha = 0$), which has the largest accuracy (no numerical diffusion) and an implicit upwind difference scheme ($\alpha = 1$), which is more robust (but more diffusive), for the propagation in σ- and θ-space.

The propagation velocities in geographical space can be obtained from the linear wave theory (see also appendix I):

$$\frac{d\underline{x}}{dt} = \underline{c}_g + \underline{U} = \frac{1}{2}\left[1 + \frac{2kd}{\sinh 2kd}\right]\frac{\sigma \underline{k}}{k^2} + \underline{U} \qquad (II.2)$$

where $\underline{c}_g$ is the group velocity in the absence of currents, $\underline{U}$ is the ambient current speed, $\underline{k}$ the wave number and d is the depth. Refraction is modelled as the propagation term in θ-domain in the energy balance equation:

$$\frac{d\theta}{dt} = c_\theta = -\frac{1}{k}\left[\frac{\partial \sigma}{\partial d}\frac{\partial d}{\partial m} + \underline{k} \cdot \frac{\partial \underline{U}}{\partial m}\right] \qquad (II.3)$$

where m is a coordinate along the wave crest. The expression for the frequency shift is:

$$\frac{d\sigma}{dt} = c_\sigma = \frac{\partial \sigma}{\partial d}\left[\frac{\partial d}{\partial t} + \underline{U} \cdot \nabla d\right] - c_g \underline{k} \cdot \frac{\partial \underline{U}}{\partial s} \qquad (II.4)$$

where s is a coordinate normal to the wave crest.

Source Terms

The right hand side of Eq. II.1 contains the source terms in terms of wave energy (and therefore needs to be divided by σ to fit into the action balance equation). It is written as the sum of a number of different source terms, representing the growth as well as the decay of wave energy. The different processes that are represented in SWAN are (Ris et al., 1995) :

- generation of wave energy by wind;
- dissipation of wave energy by whitecapping;
- dissipation of wave energy by depth induced breaking;
- dissipation of wave energy by bottom friction;
- redistribution of wave energy over the spectrum by non-linear wave-wave interactions (quadruplets and triads).

APPENDIX III: STABILITY ANALYSIS FOR THE GRADIENT APPROACH

To investigate the stability of the numerical formulations the method of Neuman is used. The analysis is carried out for the (simplified) case of constant depth and the absence of currents. Therefore the frequency shift c_σ and the refraction-induced turning rate are equal to zero. The simplified action balance equation with the gradient approach is:

$$c_x\frac{N_{x_i}-N_{x_i-1}}{\Delta x}+c_y\frac{N_{y_i}-N_{y_i-1}}{\Delta y}-\gamma\frac{(c_x\frac{N_{y_i}-N_{y_i-1}}{\Delta y})_{\theta_i+1}-(c_x\frac{N_{y_i}-N_{y_i-1}}{\Delta y})_{\theta_i-1}}{2\Delta\theta}+\gamma\frac{(c_y\frac{N_{x_i}-N_{x_i-1}}{\Delta x})_{\theta_i+1}-(c_y\frac{N_{x_i}-N_{x_i-1}}{\Delta x})_{\theta_i-1}}{2\Delta\theta}=0 \qquad (III.1)$$

The numerical formulations must fulfil the Neuman condition (Abbott and Basco, 1989):

$$|\rho|\leq 1 \qquad (III.2)$$

where ρ is the amplification factor. In the first and third sweep the waves propagate line-by-line in the y-direction, in the other sweeps the waves propagate line-by-line in the x-direction. It is sufficient to carry out the analysis for sweep one only. For the other sweeps the same stability criterion will hold (with x replaced by y and y by x).

Assuming that

$$N_{x_i,y_i,\sigma_i,\theta_i}=\hat{N}\ e^{i(px_i+q\theta_i)} \qquad (III.3)$$

$$N_{y_i+1}=\rho\ N_{y_i} \qquad (III.4)$$

where

$p = k_x \cdot \Delta x$;

$q = k_\theta \cdot \Delta\theta$;

k_x = a characteristic wave number in y-direction

k_θ = a characteristic wave number in θ-domain

the amplification factor for the gradient approach for diffraction can be written as:

$$\rho=\frac{1-i\zeta\sin q}{1+\partial(1-\cos p)-\xi\sin p\sin q+i[\partial\sin p-\zeta\sin q+\xi\sin q(1-\cos p)]} \qquad (III.5)$$

in which:

$$\partial=\frac{\Delta y}{\Delta x}\frac{c_x}{c_y} \qquad (III.6)$$

$$\xi=\frac{\Delta y}{\Delta x}\cdot\frac{\gamma}{\Delta\theta} \qquad (III.7)$$

$$\zeta=\frac{c_x}{c_y}\cdot\frac{\gamma}{\Delta\theta} \qquad (III.8)$$

The Neuman condition yields:

$$\left|\frac{1-i\zeta\sin q}{1+\partial(1-\cos p)-\xi\sin p\sin q+i[\partial\sin p-\zeta\sin q+\xi\sin q(1-\cos p)]}\right|\le 1 \qquad (III.9)$$

The Neuman condition must hold for all combinations of p and q, with $p,q \le \pi$. The propagation in geographical space is unconditionally stable. Therefore ∂ is not subjected to a stability criterion. The most severe conditions occur at the extreme directions of the different sweeps. For the directions between the two extreme directions less severe conditions will hold. For sweep one in SWAN c_x and c_y are positive and therefore the coefficients ∂, ζ and ξ as well. The extreme directions are $\theta \to 0°$ and $\theta = 90°$.

1. $\theta \to 0°$

For this direction c_y approaches zero. Therefore $\partial, \zeta \gg \xi$ and $\partial, \zeta \gg 1$ and the terms of order 1 and ξ can be neglected. The amplification factor then becomes:

$$\rho=\frac{i\zeta\sin q}{\partial(1-\cos p)+i[\partial\sin p-\zeta\sin q]} \qquad (III.9)$$

The condition for stability yields:

$$\partial(1-\cos p)-\sin p\sin q\xi\ge 0 \qquad (III.10)$$

which is most severe for $q=\pi/2$. Eq. III.10 can then be rewritten to:

$$\zeta\le\frac{1-\cos p}{\sin p}\cdot\partial \qquad (III.11)$$

For $p \to 0$ the stability condition is most severe:

$$\lim_{p\to 0}\ \zeta\le\frac{1-\cos p}{\sin p}\cdot\partial = \frac{p}{2}\cdot\partial \rightarrow \frac{\gamma}{\Delta\theta}\le\frac{k_x\,\Delta y}{2} \qquad (III.12)$$

2. $\theta = 90°$

For this direction c_x equals zero and therefore $\partial, \zeta = 0$. The amplification factor becomes:

$$\rho=\frac{1}{1-\xi\sin p\sin q+i[\xi\sin q(1-\cos p)]} \qquad (III.13)$$

Now the stability condition can be rewritten to:

$$\xi(1-\cos p)+\sin p\ge 0 \qquad (III.14)$$

which holds for all values of ξ, p and q.

For the x-direction the stability condition is similar:

$$\frac{\gamma}{\Delta\theta}\le\frac{k_y\,\Delta x}{2} \qquad (III.15)$$

The stability conditions (Eq. III.12 and III.15) are necessary conditions for a stable solution but they do not guarantee a stable solution.

It might seem surprising that a high resolution in geographical domain has a negative influence on the stability. This can be explained with Eq. III.11, which indicates that the ratio of the diffraction-induced propagation term to the geographical propagation term should be smaller than a certain value (e.g. equal to 0.13 for $p=\pi/12$). The diffraction term is a second-order term with derivatives in both spatial and directional domain. Therefore the magnitude of the aforementioned ratio is not only dependent on the resolution in θ-domain, but to the spatial resolution as well.

As mentioned before the numerical techniques in SWAN are not designed to solve higher-order differential equations. To avoid numerical instabilities a low value for γ is required. Due to the inherent distribution of wave energy over the directions, the computed wave field is smooth anyway (compared with a wave field obtained with a monochromatic model). Maybe it is better not to simulate diffraction in the whole computational domain, but to compute diffraction only locally, in areas where diffraction is dominant. This can possibly be done with a nested diffraction-refraction model, which is used in areas with strong spatial gradients only. In the other grid points the wave field is computed with the 'main model'.

APPENDIX IV: ATTEMPTS TO MAKE THE MODEL STABLE

Introduction

The basic equation that is integrated in SWAN (without the source terms) is:

$$\frac{\partial}{\partial x}[c_x N(\sigma,\theta)]+\frac{\partial}{\partial y}[c_y N(\sigma,\theta)]+\frac{\partial}{\partial \sigma}[c_\sigma N(\sigma,\theta)]+\frac{\partial}{\partial \theta}[c_\theta N(\sigma,\theta)]=0 \qquad \text{(IV.1)}$$

The numerical techniques in SWAN are specifically designed to solve this first-order differential equation. The expression for the wave number derived from the mild-slope equation contains second-order spatial derivatives of the wave amplitude. Using these second-order derivatives to compute c_θ results in third-order derivatives. Adding the third-order diffraction term made the model numerically unstable. It appeared that instability already arises in areas where the wave field is not disturbed by obstacles. The instability might be influenced by: (a) the spatial resolution, (b) the formulation for the second-order spatial derivatives and (c) the formulation for the turning rate c_θ. The following attempts are made to obtain a stable solution.

Spatial resolution

Since diffraction effects play an important role on a scale of only a few wavelengths the initial spatial grid was chosen a quarter of the mean wave length. Decreasing the resolution (i.e. increasing the step interval Δx and Δy) improved the stability slightly. Only for step intervals of the magnitude of two wavelengths or more the computations became stable. For these step intervals the second-order spatial derivatives have become negligible. The results of these (stable) computations were about the same as those made with the original formulation for the action balance equation.

Formulation for the second-order derivatives

In the expression for the wave number the wave amplitude appears in the denominator. Therefore the diffraction term cannot be computed correctly at places where the wave amplitude equals zero. This can be the case in the geographical domain (immediately behind the breakwater), but also in spectral space at the boundaries of the spectrum. For this reason the wave amplitude in the denominator is expressed as:

$$N_{x_i} = \frac{N_{x_i-1}+2N_{x_i}+N_{x_i-1}}{4} \quad \textit{and} \quad N_{y_i} = \frac{N_{y_i-1}+2N_{y_i}+N_{y_i+1}}{4} \qquad \text{(IV.2)}$$

A second attempt to prevent 'dividing by zero' was made by taking an absolute minimum for the value in the denominator. Thirdly the diffraction term is computed only for spectral bins that contain a minimum amount of energy, e.g. more than a thousandth of the maximum amount for that particular frequency and that geographical grid point (thus a relative minimum). These alternative formulations for the second-order derivatives had no influence on the stability of the computations.

Formulation for the turning rate c_θ

Since the second-order derivatives of the wave amplitude remained limited (and the wave number **K** as well) the instability seemed to be caused by the formulation for the (diffraction-induced) turning rate. Therefore it seemed meaningful to limit this propagation speed. To do so a Courant number (CFL) for propagation in directional domain is used:

$$CFL = \frac{\frac{c_\theta}{\Delta\theta}}{|\frac{c_x}{\Delta x}| + |\frac{c_y}{\Delta y}|} \qquad \text{(IV.3)}$$

With this Courant number a maximum value for c_θ is determined:

$$c_{\theta_{max}} = CFL_{max} \cdot \Delta\theta \cdot [|\frac{c_x}{\Delta x}| + |\frac{c_y}{\Delta y}|] \qquad \text{(IV.4)}$$

The propagation speed is computed as:

$$\begin{aligned} c_\theta &= \frac{c_g}{K}\frac{\partial K}{\partial m} \quad for \quad CFL \le CFL_{max} \\ c_\theta &= c_{\theta_{max}} \quad for \quad CFL > CFL_{max} \end{aligned} \qquad \text{(IV.5)}$$

The initial value for CFL_{max} was chosen equal to one. For this value for CFL_{max} there was no influence on the stability. Decreasing CFL_{max} (and consequently $c_{\theta,max}$) showed an improvement. However the results were stable only when the value for CFL_{max} was so low ($\le$ 0.01) that the turning rate c_θ became negligible.

A last attempt was made by computing the wave field in the first iteration with the gradient approach to create a smoothed wave field. The results of these computations were used to compute the wave field with the mild-slope approach. There was no effect on the stability of the computations.

Conclusions

It seemed that the abovementioned attempts to influence the stability of the computations were not enough to obtain stable solutions. The solution of the third-order differential equation with the mild-slope approximation for diffraction requires other numerical techniques than those used in SWAN.

APPENDIX V: THE SOMMERFELD-SOLUTION

An analytical solution for diffraction is derived by Sommerfeld (1896) for the case of a semi-infinite breakwater. In case of diffraction energy is transferred laterally along a wave crest. Therefore the phase function becomes of importance and it is no longer allowed to use the phase-averaged wave properties. Analytical solutions for diffraction can be obtained after making the following assumptions (in addition to those made in the linear wave theory):

- The depth is constant;
- The obstacle, around which the waves diffract, is supposed to extend vertically from the bottom through the free surface, and to be rigid and impermeable (and therefore 100% reflective);
- The thickness of the screen or the width of the breakwater is theoretically zero and has a highly idealized geometry.

Using a potential formulation (Eq. I.3), which has to meet the Laplace equation (Eq. I.1) the following Helmholtz equation in two dimensions can be derived:

$$\frac{\partial^2 G}{\partial x^2}+\frac{\partial^2 G}{\partial y^2}+k^2 G=0 \qquad \text{V.1}$$

in which

$$G(x,y)=\frac{a(x,y)}{a_\infty}e^{i\psi(x,y)} \qquad \text{V.2}$$

Two boundary conditions are needed to represent the breakwater:

$$\frac{\partial G}{\partial \eta}=0 \qquad \text{V.3}$$

$$G \rightarrow e^{-iky'}$$

in which η(x,y,t) is the instantaneous elevation of the water surface. See Figure V.1 for the definition of the coordinate system used.

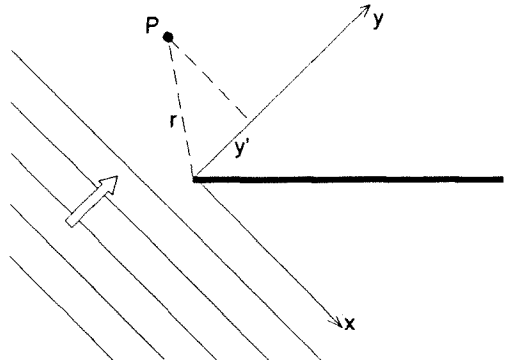

Figure V.1 Definition of coordinate system

Sommerfeld derived an analytical solution for a semi-infinite impermeable breakwater located at the positive x-axis. 'Semi-infinite' means that the breakwater (in the direction of the positive x-axis) extends sufficiently far to neglect the influence of the waves diffracting at the other breakwaterhead and that the wave field at the negative x-axis is not disturbed by other wave sources than incident wave field.

The Sommerfeld-solution contains a term for the reflected wave and one for the incident wave field (see Figure V.2).

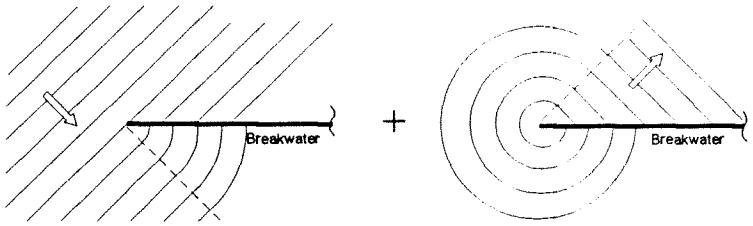

Figure V.2 Diffraction caused by incoming and by reflected waves

The influence of the reflected wave behind the breakwater is relatively small and can therefore be neglected. The remaining Sommerfeld solution contains an integral with a complex integrand:

$$G(x,y)=e^{-iky}\frac{e^{i\frac{\pi}{4}}}{\sqrt{2}}\int_{-\infty}^{\pm 2\sqrt{\frac{r-y'}{L}}} e^{-i\frac{\pi}{2}s^2}ds \qquad \text{V.4}$$

with $r=(x^2+y^2)^{1/2}$ and $L=2\pi/k$.

The integral can be split into a real and an imaginary part:

$$\int_{-\infty}^{N} e^{-i\frac{\pi}{2}s^2}ds=\int_{-\infty}^{0}\cos(\frac{\pi}{2}s^2)ds-i\int_{-\infty}^{0}\sin(\frac{\pi}{2}s^2)ds+\int_{o}^{N}\cos(\frac{\pi}{2}s^2)ds-i\int_{0}^{N}\sin(\frac{\pi}{2}s^2)ds=(\frac{1}{2}-\frac{1}{2}i)+c(N)-is(N) \qquad \text{V.5}$$

The resulting four integrals are also known as the Fresnel integrals.

$$c(x)=\int_{0}^{x}\cos(\frac{\pi}{2}s^2)ds \qquad Lim_{x\to\infty}c(x)=\frac{1}{2}$$

$$s(x)=\int_{0}^{x}\sin(\frac{\pi}{2}s^2)ds \qquad Lim_{x\to\infty}s(x)=\frac{1}{2} \qquad \text{V.6}$$

Now G(x,y) can be calculated and therefore the diffraction factor K_D (x,y), which is defined as:

$$K_D=\frac{a(x,y)}{a_\infty}=|G(x,y)| \qquad \text{V.7}$$

and in which a_∞ is the amplitude of the undisturbed incident wave.

The solution can qualitatively be explained by using Huygens' principle, which says that an advancing wave front can be considered as a sequence of elementary wave sources, each of which radiates energy in a circular pattern (see Figure V.3). The wave disturbance at some point P can be determined by adding the contributions from the various sources which can reach the point. If this summation is carried out over all the sources from $-\infty$ to $+\infty$ the undisturbed, incident wave motion is recovered.

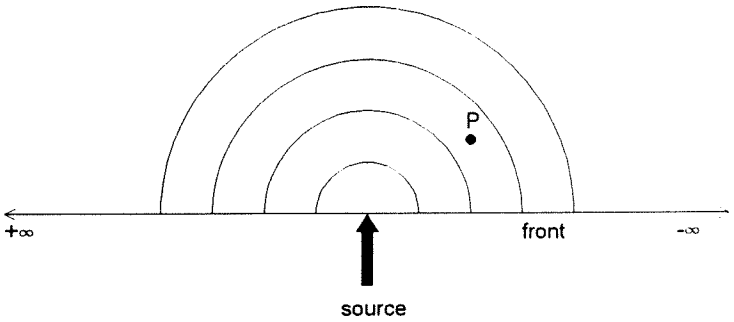

Figure V.3 Huygens' principle.

For a point behind a breakwater the summation is carried out over those sources which can reach the point by wave rays.